JOURNAL OF GEOPHYSICAL RESEARCH, VOL. 106, NO. D14, PAGES 14,783-14,803, JULY 27, 2001

Hypothesized climate forcing time series for the last 500 years

A. Robertson,[1] J. Overpeck,[2] D. Rind,[3] E. Mosley-Thompson,[4] G. Zielinski,[5] J. Lean,[6] D. Koch,[3] J. Penner,[7] I. Tegen,[3] and R. Healy[3,8]

Abstract. A new compilation of annually resolved time series of atmospheric trace gas concentrations, solar irradiance, tropospheric aerosol optical depth, and stratospheric (volcanic) aerosol optical depth is presented for use in climate modeling studies of the period 1500 to 1999 A.D. Atmospheric CO_2, CH_4, and N_2O concentrations over this period are well established on the basis of fossil air trapped in ice cores and instrumental measurements over the last few decades. Estimates of solar irradiance, ranging between 1364.2 and 1368.2 W/m^2, are presented using calibrated historical observations of the Sun back to 1610, along with cosmogenic isotope variations extending back to 1500. Tropospheric aerosol distributions are calculated by scaling the modern distribution of sulfate and carbonaceous aerosol optical depths back to 1860 using reconstructed regional CO_2 emissions; prior to 1860 the anthropogenic tropospheric aerosol optical depths are assumed to be zero. Finally, the first continuous, annually dated record of zonally averaged stratospheric (volcanic) optical depths back to 1500 is constructed using sulfate flux data from multiple ice cores from both Greenland and Antarctica, in conjunction with historical and instrumental (satellite and pyrheliometric) observations. The climate forcings generated here are currently being used as input to a suite of transient (time dependent) paleoclimate model simulations of the past 500 years. These forcings are also available for comparison with instrumental and proxy paleoclimate data of the same period.

1. Introduction

There has been increasing concern over the past few decades regarding potential effects humans may exert on the climate system. The possible consequences of anthropogenic climate forcing are significant and include substantial ecological and societal effects [*Houghton et al.*, 1996], as well as extra challenges to climate prediction efforts. Unfortunately, attribution of any observed climatic change to anthropogenic forcing is complicated by the fact that human-induced change will be superimposed on natural climate variability.

Numerical models such as general circulation models (GCMs) and climate system models are currently considered the most advanced technology we have to anticipate future climate changes on interannual to centennial timescales. However, before results from numerical models can be considered accurate predictors of future change, we must demonstrate their ability to simulate in a realistic manner the full range of atmosphere and atmosphere-ocean variability. The merit of numerical models can be demonstrated through the comparison of modern climate simulations with modern climate data. However, as most models are tuned to modern climate, it is difficult to tell if such a model will simulate realistic climate change in response to altered radiative forcing. Also, models must be able to simulate time-dependent variability that is not present in the brief "snapshot" of modern climate provided by instrumental and satellite data alone. It is therefore critical to compare paleoclimatic observations with paleoclimate simulations for the same periods of time. When this is done, the full range of potential future climate change can be better understood and predicted.

Over the decade to century timescales of climate change, there are a number of hypothesized forcing mechanisms. *Rind and Overpeck* [1993] used model results to suggest that important sources of climate variability on the decade to century timescale include (1) natural variability in the atmosphere; (2) natural variability in ocean circulation (e.g., El Niño-Southern Oscillation (ENSO), North Atlantic Deep Water (NADW formation); (3) solar variability (e.g., the maunder minimum); (4) variability in volcanically derived stratospheric aerosols; and (5) atmospheric trace gas variability. Additionally, *Overpeck et al.* [1997] and *Mann et al.* [1998] have used atmospheric trace gas, solar, and stratospheric aerosol variability in empirical efforts to explain observed changes in paleoclimate proxy reconstructions covering the last few centuries; *Lean et al.* [1995] have also estimated that solar forcing may have

[1]Institute of Arctic and Alpine Research and Department of Geological Sciences, University of Colorado, Boulder.
[2]Institute for the Study of Planet Earth and Department of Geosciences, University of Arizona, Tucson.
[3]NASA Goddard Institute for Space Studies, New York.
[4]Byrd Polar Research Center, The Ohio State University, Columbus.
[5]Climate Studies Center, Institute for Quaternary Studies, University of Maine, Orono.
[6]E.O. Hulburt Center for Space Research, Naval Research Laboratory, Washington, D.C.
[7]Department of Atmospheric, Oceanic, and Space Sciences, University of Michigan, Ann Arbor.
[8]Woods Hole Oceanographic Institute, Woods Hole, Massachusetts.

Paper number 2000JD900469.
0148-0227/01/2000JD900469$09.00

contributed about half of the observed warming since 1860. In addition to the above mentioned forcings, there are many other potential climate forcings that can affect climate on the decade to century timescale. The direct radiative effect of anthropogenically derived tropospheric aerosols can alter the amount of radiation incident upon the surface of the Earth through both reflection and absorption [*Schimel et al.*, 1996]. The indirect radiative effect of tropospheric aerosol loading can lead to an increased number of cloud condensation nuclei (CCN), altering the radiative properties of clouds [*Schimel et al.*, 1996]. Other hypothesized climate forcings on the decade to century timescale include tropospheric mineral dust aerosols [*Overpeck et al.*, 1996; *Tegen et al.*, 1996]. Orbital forcing is also well known as a significant climate forcing mechanism, operating over centennial to millennial timescales [*Berger and Loutre*, 1991]. Finally, land cover change can affect surface albedo, atmospheric circulation, and moisture transport at the boundary layer [*Rind*, 1984; *Woodward et al.*, 1995; *TEMPO*, 1996].

The goal of this paper is to present a compilation of time series of hypothesized climate forcings for the past 500 years. We choose to present the forcings that are presumed to be the most important mechanisms for climate change on timescales of decades to centuries. We present high-resolution time series of trace gas (CO_2, CH_4, N_2O), stratospheric (volcanically derived) aerosol, and solar climate forcings for the period 1500 to the present, as well as tropospheric aerosol (from both fossil fuel and biomass burning) forcing for the industrial period (1860 to present). We describe how these forcing series were reconstructed and evaluate their usefulness and potential climate implications. Our compilation is the first created explicitly for numerical model simulations and is now being used as input for a suite of paleoclimate model simulations being carried out using the NASA GISS GCMs II and II'. These climate-forcing time series will all be available at the World Data Center A for Paleoclimatology in Boulder, Colorado (http://www.ngdc.noaa.gov/paleo/).

2. Reconstruction of Climate Forcings

2.1. Trace Gases (1500 to Present)

Changing trace gas concentrations are probably one of the most widely debated climate forcings. Greenhouse gases, including CO_2, CH_4, and N_2O, are relatively transparent to incoming solar radiation but absorb outgoing longwave radiation. Varying atmospheric concentrations of trace gases (i.e., from fossil fuel combustion, deforestation, increased evaporation, degassing of sea water) will presumably modify the balance between incoming and outgoing radiation, potentially initiate several positive feedbacks, and result in a change in the temperature of the Earth and the atmosphere [*Schimel et al.*, 1996]. Trace gases such as halocarbons and tropospheric ozone also result in a positive radiative forcing; also, CO_2-induced stratospheric cooling is expected to result in decreases in stratospheric ozone, altering the amount of ultraviolet radiation reaching the surface of the Earth [*Shindell et al.*, 1998]. However, these trace gases are not included here due to the relatively small net radiative effects of halocarbons prior to the 1970s and the low confidence regarding the net radiative effect associated with changes in tropospheric and stratospheric ozone [*Schimel et al.*, 1996].

Comparison of ice core and instrumental trace gas data indicates that glacial ice offers a reliable method of determining past atmospheric concentrations of trace gases [*Lorius et al.*, 1985; *Raynaud and Barnola*, 1985; *Barnola et al.*, 1987; *Neftel et al.*, 1988]. The firnification of snow deposited on an ice sheet traps air bubbles in the ice. Methods have been developed which allow these bubbles to be sampled in the laboratory without contamination and thus make direct measurements of the fossil air. However, there are multiple sources of potential error, some of which include inaccuracies in the age model associated with a particular ice core; contamination associated with natural ice melting; inaccurate determination of the time lag between the deposition of the snow and the enclosure of the air bubbles; mixing with the modern atmosphere due to postcoring problems such as melting and core fracture; incorporation of air bubbles into the molecular structure of the ice due to extremely high pressures [*Etheridge et al.*, 1996]. The reliability of trace gas concentrations measured from fossil air trapped in glacial ice can be estimated by comparison with direct instrumental trace gas mixing ratio measurements that have been made since 1957 at various stations around the world [*Dlugokencky et al.*, 1994; *Keeling and Whorf*, 1994; *Prinn et al.*, 1994].

The Antarctic Law Dome ice core has been used [*Etheridge et al.*, 1996] to produce the highest resolution CO_2 record to date for the period 1500 to 1969, a record that compares well during the period of overlap with the instrumental CO_2 data from Mauna Loa (Figure 1a); as CO_2 is well mixed between the Northern and the Southern Hemispheres over decade to century timescales [*Etheridge et al.*, 1996], this Antarctic record can apply to the entire globe. A cubic spline was fit to the ice core data to estimate annually resolved data. The increase in CO_2 concentration after the industrial revolution is clearly seen after 1850. The current (1997) CO_2 concentration is 363.8 ppmv and has been increasing at a rate of 1.75 ppmv (0.48%) per year (Table 1).

The Antarctic Mizuho ice core has been used in conjunction with the Greenland Site J ice core [*Nakazawa et al.*, 1993] to produce a high-resolution CH_4 record for the period 1500 to 1951; instrumental CH_4 data are available from 1984. Because CH_4 is not so well mixed between the Northern and the Southern Hemispheres as CO_2 [*Nakazawa et al.*, 1993], records from both hemispheres were needed to develop a series of average global values to which a cubic spline could be fit to estimate an annually resolved time series. A cubic spline was also used to fill in the 33-year gap between the end of the ice core record (1951) and the beginning of the instrumental record (1984; Table 1). Clearly seen is the increase in concentration after the industrial revolution (Figure 1b). The current (1997) CH_4 concentration is 1750.8 ppbv and has been increasing at a rate of 4.11 ppbv (0.23%) per year (Table 1).

Because of the high variability seen in available N_2O records (Figure 1c), we chose to use a compilation of multiple records from Antarctica to derive the final forcing time series. The interhemispheric gradient of atmospheric N_2O concentration was estimated to be less than 1 ppbv [*Khalil and Rasmussen*, 1988], suggesting that the Antarctic ice core data would be representative of global atmospheric conditions. The Antarctic Byrd Station [*Khalil and Rasmussen*, 1988], Law Dome [*Etheridge et al.*, 1988], and Adelie Land [*Zardini et al.*, 1989] ice cores were all used to produce a high-resolution N_2O record for the period 1500 to 1966; instrumental N_2O data are available from 1984 [*Prinn et al.*, 1994]; a polynomial was then fit through all four data series (Figure 1c). The higher variability seen in the N_2O record was attributed to differences in analytical techniques among the three sample sets and the

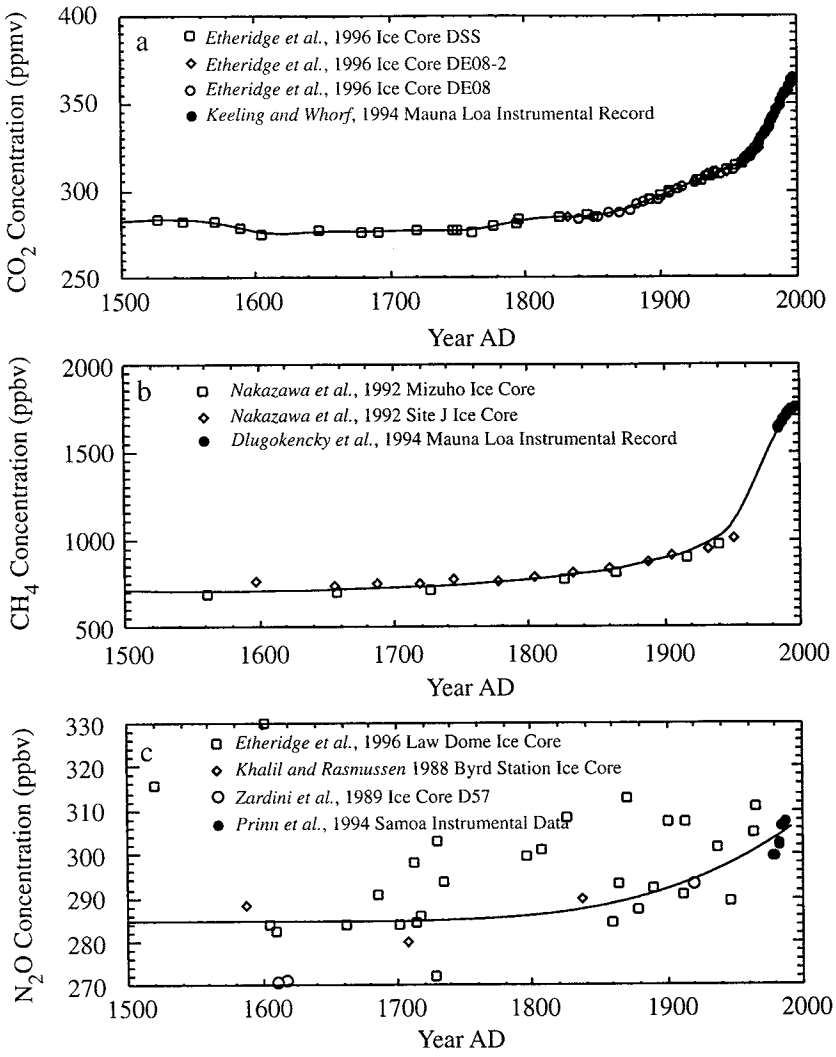

Figure 1. Time series of globally averaged atmospheric mixing ratios of CO_2, CH_4, and N_2O. Our final CO_2 and CH_4 trends are a cubic spline that was fit to both ice core data and instrumental data. The N_2O trend is a best fit polynomial based on ice core data and instrumental data. See Table 1 for original data references and sources. Estimated annual trace gas concentrations associated with each spline are available at http://www.ngdc.noaa.gov/paleo/.

use of different calibration gases [*Zardini et al.*, 1989]. The current (1997) N_2O concentration is 306.4 ppbv and has been increasing at a rate of .21 ppbv (0.07%) per year (Table 1).

2.2. Tropospheric Aerosols (1860 to Present)

Tropospheric aerosols derived from biomass burning, industrial sources, and natural sources are a potentially important climate forcing component, due to their ability to alter the amount of insolation reaching the surface of the Earth. Sulfate aerosols can backscatter solar radiation, increasing the planetary albedo, and cooling the surface; darker aerosols, such as black carbon, can also absorb radiation, resulting in atmospheric heating [*Penner et al.*, 1992, 1994; *Tegen et al.*, 1997]. The relative amounts of radiative absorption or backscatter caused by a particular aerosol can be quantified using the single-scattering albedo (ω), which is defined as the ratio of scattered radiation to the sum of scattered and absorbed radiation [*Schimel et al.*, 1996]. A single-scattering albedo of 1 scatters all incident radiation; a single-scattering albedo of zero absorbs all incident radiation. Many complexities are present on regional and local spatial scales, based on the varying size and composition of aerosols from different sources. Tropospheric aerosols are spatially weighted toward the general region from which they were emitted, due to their short atmospheric residence time. In some highly industrialized regions the negative direct-radiative forcing of tropospheric aerosols may counter the positive radiative forcing due to elevated concentrations of greenhouse gases [*Mitchell and Johns*, 1997]. The indirect radiative effect of tropospheric aerosol loading can also lead to an increased number of cloud condensation nuclei (CCN), altering the radiative properties of clouds through increased cloud persistence and cloud optical thickness [e.g., *Charlson et al.*, 1992; *Langner et al.*, 1992; *Curry et al.*, 1996]. Tropospheric aerosols may also be important in modifying atmospheric chemistry [*Koch et al.*, 1999].

Modern tropospheric aerosol optical depth estimates from nonnatural aerosols are a function of sulfate and carbonaceous

Table 1. Summary of Parameters Related to Ice Core and Instrumental Records of CO_2, CH_4, and N_2O

Ice Core Record	CO_2	CH_4	N_2O
Ice core location(s)	Law Dome, Antarctica	Mizuho, Antarctica	Byrd Station, Antarctica
		Site J, Greenland	Law Dome, Antarctica
			Adelie Land, Antarctica
Number of ice cores:	3	2	3
Period of ice core records	1840-1969 A.D.	1310-1940 A.D.	1688-1838 A.D.
	1832-1978 A.D.	1598-1951 A.D.	1520-1966 A.D.
	1006-1959 A.D.		1612-1919 A.D.
Ave. sampling resolution[a]:	4.2 years	78.8 years	75.0 years
	14.6 years	29.4 years	11.4 years
	23.8 years		153.5 years
References	*Etheridge et al.* [1996]	*Nakazawa et al.* [1993]	*Khalil and Rasmussen* [1988]
			Etheridge et al. [1988]
			Zardini et al. [1989]

Instrumental Record	CO_2	CH_4	N_2O
Sampling location	Mauna Loa	Mauna Loa	Samoa
Period of record	1959-1998 A.D.	1984-1998 A.D.	1979-1989 A.D.
Source	ftp://ftp.cmdl.noaa.gov/ccg /co2/in-situ/mlo/	ftp://ftp.cmdl.noaa.gov/ccg /ch4/in-situ/mlo/	*Prinn et al.* [1994]

Final Record	CO_2	CH_4	N_2O
Preindustrial concentration	286.3 ppmv	836.9 ppbv	288.8 ppbv
Modern (1997) concentration	363.8 ppmv	1750.8 ppbv	306.4 ppbv
Current rate of increase	1.75 ppmv (0.48 %)/yr	4.11 ppbv (0.23 %)/yr	0.21 ppbv (0.07 %)/yr

[a] Average sample spacing for each ice core used.

aerosols derived from both fossil fuel combustion and biomass burning, in addition to mineral dust aerosols entrained following land cover modification. Modern tropospheric aerosol optical depth estimates from natural aerosols are a function of sulfate aerosols emitted from volcanoes and DMS production, entrainment of mineral dust aerosols from naturally occurring source regions [e.g., *Tegen and Fung*, 1994], and photochemical conversion of gaseous emissions from plants [*Liousse et al.*, 1996]. The modern tropospheric sulfate aerosol optical depth distribution, shown in Plate 1a, was based on model results from *Koch et al.* [1999], who modeled sulfur species on-line in the GISS GCM model II' to estimate the transport and removal of both natural and anthropogenic sulfate aerosols based on 1985 emissions. *Koch et al.* [1999] considered natural sources of sulfate in the form of dimethylsulfide (DMS) and noneruptive volcanoes as well as anthropogenic sources of sulfate from fossil fuel combustion (based on 1985 Global Emissions Inventory Activity (GEIA) emissions), biomass burning, and aircraft emissions. Modeled sulfate was removed from the atmosphere through both wet and dry deposition [*Koch et al.*, 1999]. Plate 1b shows the modern tropospheric carbonaceous aerosol optical depth distribution from *Liousse et al.* [1996], who used 1980 emissions of both black and organic carbon particles from biomass burning and fossil fuel combustion sources. These aerosol sources were then incorporated into a transport model which used the precipitation and wind fields from the Community Climate Model (CCM1) to model the transportation and deposition of the aerosols [*Liousse et al.*, 1996]. Finally, the modern tropospheric mineral dust aerosol loading distribution (Plate 1c) was based on model results from *Tegen et al.* [1997], who calculated dust uplift on the basis of calculated soil moisture, surface wind speed, soil texture, and soil surface conditions from both natural and disturbed sources. Atmospheric loading was then calculated using model-derived wind speed and precipitation patterns from the GISS II' GCM, with both wet and dry deposition of the aerosols.

On the basis of the hypothesis that time-dependent patterns of anthropogenic tropospheric aerosol optical depth closely follow CO_2 emissions, we used regional CO_2 emission data for the nine different regions of the world defined by *Marland et al.* [1994] (Figure 2) as a proxy for anthropogenic aerosol emissions over time. The use of regional emission data rather than globally averaged data takes into account spatial differences of development and industrialization. The only

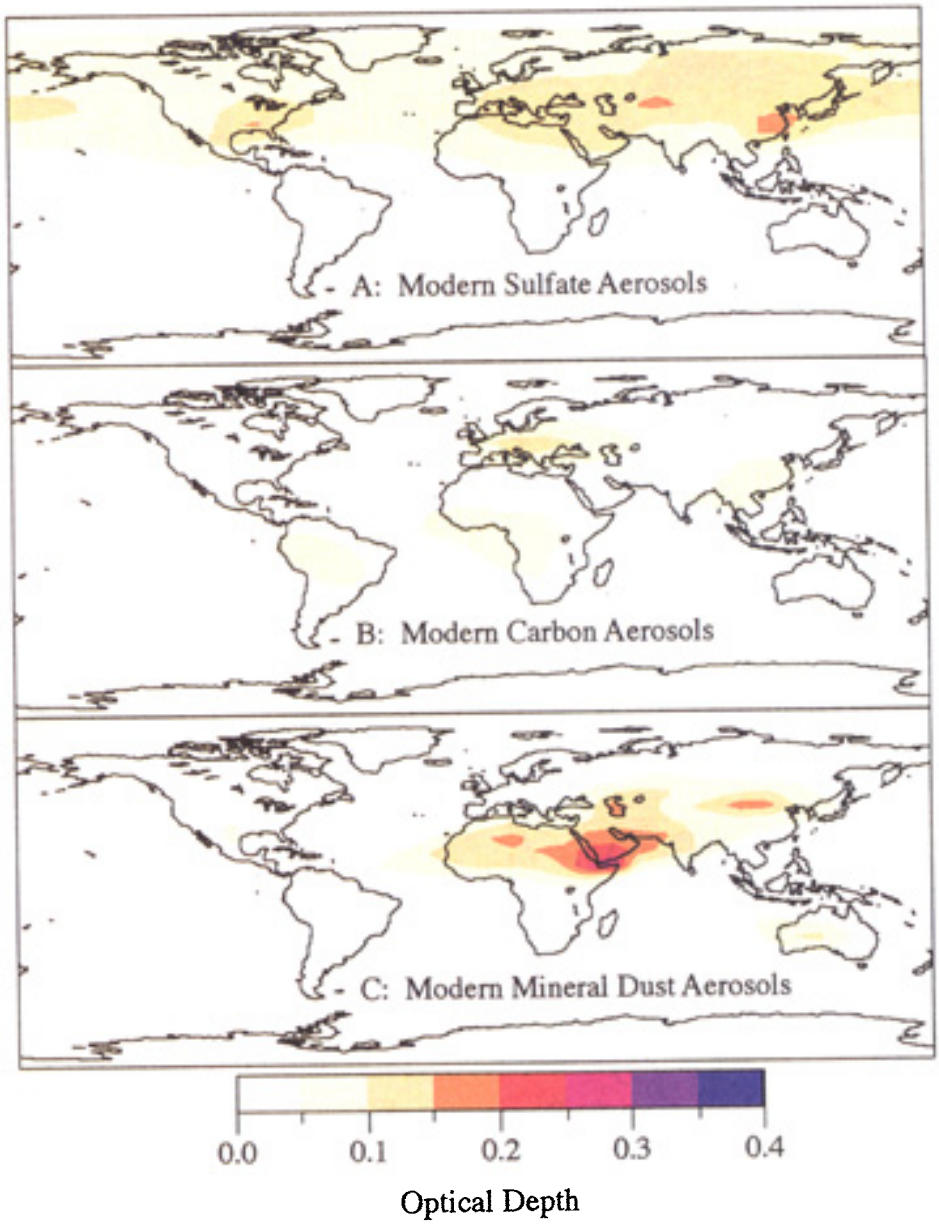

Plate 1. Plate 1a shows the modern distribution of sulfate aerosol optical depth based on model results from *Koch et al.* [1999], who used the GISS model II wind and precipitation fields to model the transport and removal of both natural and anthropogenic sulfate aerosols. Plate 1b shows the modern carbonaceous aerosol loading distribution from *Liousse et al.* [1996], who incorporated 1980 emissions of both black and organic carbon particles from biomass burning and fossil fuel combustion sources into a transport model which used the precipitation and wind fields from the Community Climate Model (CCM1) to model the transportation and deposition of the aerosols. The modern mineral dust aerosol optical depth distribution (Plate 1c) was based on model results from *Tegen et al.* [1997], who calculated dust uplift based on calculated soil moisture, surface wind speed, soil texture, and soil surface conditions from both natural and disturbed sources. Atmospheric loading was then calculated using model-derived wind speed and precipitation patterns, with wet and dry deposition of the aerosols.

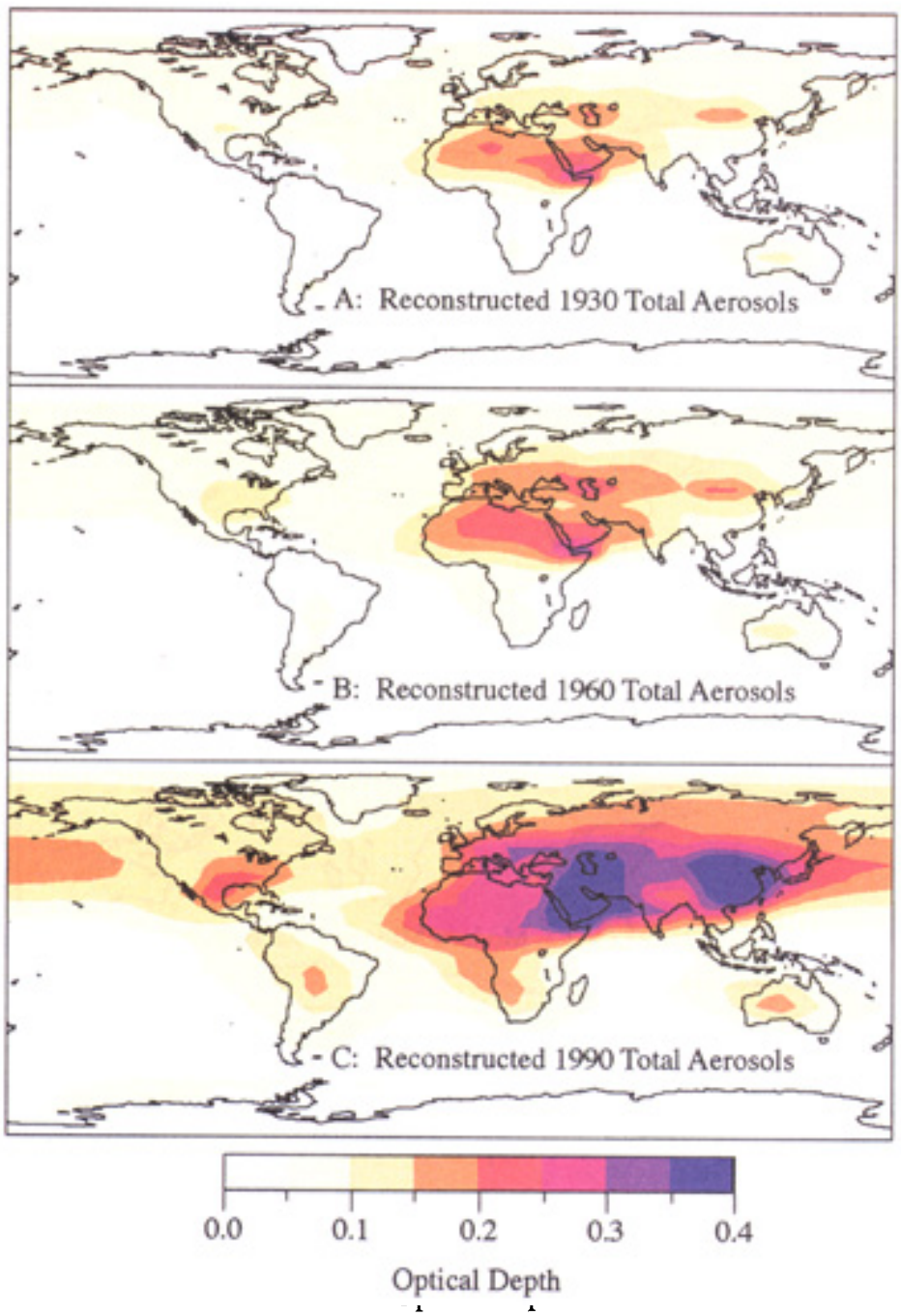

Plate 2. Reconstructed global optical depth distributions due to tropospheric carbonaceous, sulfate, and mineral dust aerosols for (a) 1930, (b) 1960, and (c) 1990. The regional emission curves in Figure 2 were used to scale the modern distributions of anthropogenically derived tropospheric aerosol optical depth (Plate 1); the mineral dust aerosol loading was held constant. Annual gridded global arrays of estimated tropospheric aerosol optical depth are available at http://www.ngdc.noaa.gov/paleo/.

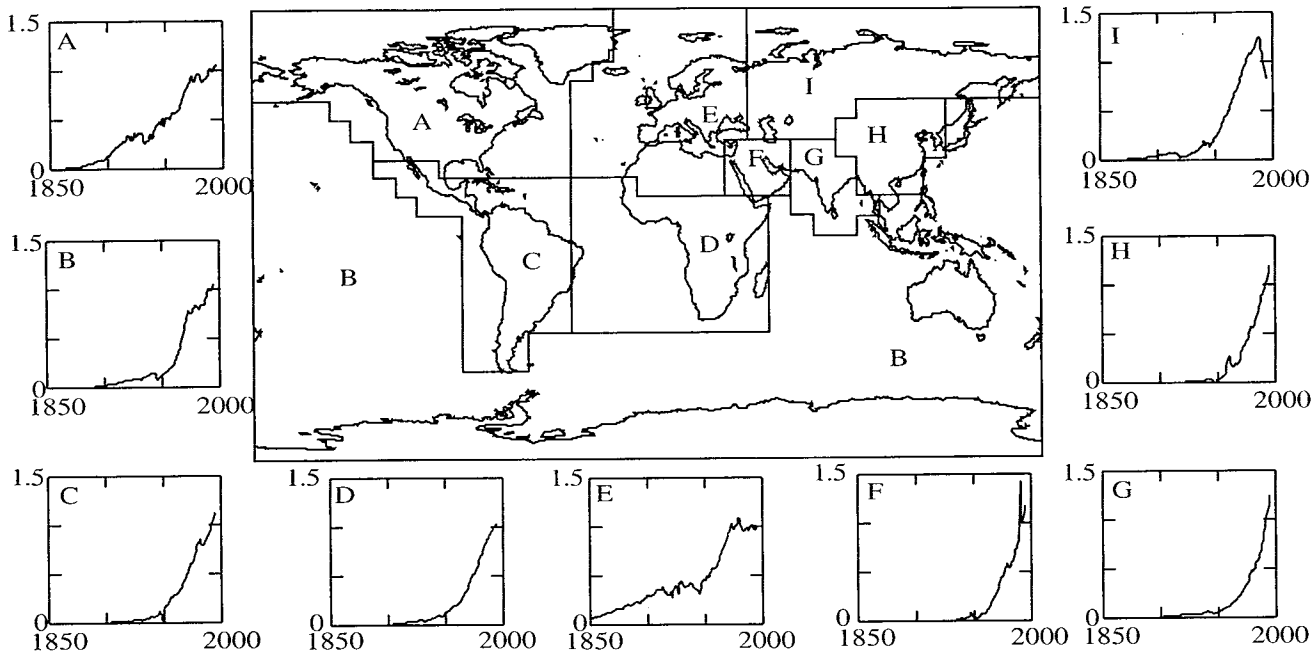

Figure 2. Time-varying global tropospheric aerosol optical depth distributions were created by scaling the modern distribution of anthropogenic tropospheric aerosol optical depth back to 1860 using regional CO_2 emission estimates. Shown here are the ratios of CO_2 emissions data for nine different regions of the world [*Marland et al.*, 1994], expressed in ratios relative to 1992 values. These time dependent CO_2 emission ratios were used to scale the modern values downward for past years. A regional scaling was used because different areas of the globe followed different temporal patterns of industrialization. The regions used are as follows: (a) North America, (b) Oceania, (c) developing America, (d) Africa, (e) western Europe, (f) Middle East, (g) Far East, (h) centrally planned Asia, (i) eastern Europe (modified from *Marland et al.* [1994]).

modification made to the regional divisions created by *Marland et al.* [1994] was the extension of the western Europe region into northern Africa (Figure 2), as much of the modern northern Africa anthropogenic aerosol load appeared to be predominantly affected by emissions from western Europe. Time-dependent CO_2 emission ratios relative to 1992 (Figure 2 time series) were then calculated for each region from the *Marland et al.* [1994] data; these ratios were then used to standardize the modern (1980 and 1985 for carbonaceous and sulfate, respectively) anthropogenic optical depth distributions to 1992 values and to, subsequently, scale these values downward back to 1860. Because of the changing relationship between CO_2 emissions and tropospheric aerosol emissions (due to increasing efficiency of fossil fuel combustion) these CO_2 emission curves probably result in a maximum estimate of the amplitude of anthropogenic tropospheric aerosol increase since 1860. Prior to 1860 the anthropogenic component of the aerosol loading was set to zero, because the anthropogenic emissions that were originally used as model input to calculate the modern aerosol loading were probably insignificant. However, there probably has been variability in biomass burning prior to 1860 [*Robock and Graf*, 1994]; the time and space distributions of these aerosol loadings are not currently well constrained and are therefore not considered here. Finally, we are also not able to account here for natural variability of sulfate (from DMS and noneruptive volcanoes) and mineral dust components of tropospheric aerosol loading; optical depths associated with these aerosols were therefore kept constant over the course of our reconstruction. However, we acknowledge the potential for regionally varying wind velocities and volcanic activity to alter the atmospheric load for these aerosol types.

The reconstructed total tropospheric optical depth distributions of anthropogenic and natural aerosols for three years, 1930, 1960, and 1990 (Plate 2), illustrate the time-dependent patterns of change in tropospheric optical depth associated with different regions of the globe. Plate 2 incorporates the varying levels of anthropogenic aerosols calculated from the regional trends in Figure 2 as well as constant levels of mineral dust and natural sulfate. Industrially derived aerosols are primarily confined to the Northern Hemisphere; aerosols derived from biomass burning are primarily confined to equatorial regions and the Southern Hemisphere. Regions with areas of high mineral aerosol loading include the Sahara desert, the Arabian Peninsula, and

Table 2. Globally Averaged Tropospheric Aerosol Optical Depth Estimates

Aerosol Type	This Study (1990 Values)	*Andreae* [1995]
Anthropogenic H_2SO_4	0.046	0.032
Natural H_2SO_4	0.012	0.024
Total carbon	0.029	0.033
Mineral dust	0.026	0.023

the Gobi desert. The total annually averaged optical depth peaks at 0.48 in the highly industrialized area of eastern China, due primarily to high sulfate and carbonaceous aerosol loading. The total annually averaged optical depth peaks at 0.45 in the Middle East, due to high levels of sulfate and mineral dust aerosol loading.

As shown in Table 2, globally averaged tropospheric aerosol estimates from the compilation presented here compare well with estimates presented by *Andreae* [1995]. Both the mineral dust aerosol optical depths and the total carbon (organic carbon and black carbon) aerosol optical depths differ by less than 0.005. We estimate the anthropogenic sulfate optical depths to be a bit higher (about 0.014 (43%)) relative to those calculated by *Andreae* [1995]; this is compensated by our slightly lower (about 0.012 (50%)) estimate of natural sulfate optical depths relative to those calculated by *Andreae* [1995]. Our globally averaged tropospheric aerosol optical depth estimate for 1990 from all sulfate, carbon, and mineral dust sources is 0.113; *Andreae* [1995] calculated a comparable estimate of 0.112.

2.3. Solar Irradiance (1500 to Present)

The Sun is the primary driver of the climate system, emitting most of its energy as visible radiation (0.4-0.7 μm), with lesser amounts in the ultraviolet and infrared range. The solar constant is currently about 1368 W/m^2, but this value may vary by up to 0.4% on timescales of decades to centuries [*Hoyt and Schatten,* 1993; *Lean et al.*, 1995]. The primary source of solar variability on these timescales is believed to be variability in the Sun's magnetic field. *Spruitt* [1994] describes the magnetically induced variability as being resultant of one of two processes. First, during the growth of a magnetic field, kinetic energy is transformed into magnetic energy, resulting in a net loss of available thermal energy; the opposite happens during the decay of the magnetic field. Secondly, an existing magnetic field at the boundary of the Sun's core and convection zone can interfere with thermal convection. The former process only happens when magnetic fields are created or destroyed; the latter can happen whenever there is an existing magnetic field. Magnetic fields are regulated by the reversal of the solar magnetic poles, which happens on a 22-year (Hale) cycle [*Beer et al.*, 1996].

Sunspots are the most conspicuous aspect of solar variability. They form as a result of a magnetic flux tube penetrating the photospheric (visible) layer of the Sun. They appear as dark spots on the surface of the Sun, due to their inhibition of convection of thermal energy to the photosphere, and are therefore cooler than the rest of the surface of the Sun. Sunspots vary according to the 22-year Hale cycle that describes the reversal of the magnetic poles of the Sun. However, simple observations of sunspots cannot differentiate between positive and negative polarity; sunspots therefore appear to vary according to the 11-year (Schwabe) cycle [*Beer et al.*, 1996].

Recent attempts to link climate change with solar variability were made by *Eddy* [1976] and *Eddy et al.* [1982] who used both historical observations and spacecraft measurements to identify variations in the total radiative output of the Sun of 0.1 to 0.3%. *Eddy* [1976] performed an exhaustive review of the historical literature to demonstrate that the maunder minimum (1645-1715) was real and not an artificial result of poor observations. In his subsequent paper, *Eddy et al.* [1982] looked at solar variability over the last 100 years and found that variations of up to 0.5% can occur on timescales of days to weeks, with lower variability of the order of 0.1% occurring on timescales of years.

Geologic proxy data have also been used in an attempt to understand past variability of solar irradiance. *Stuiver* [1980] and *Stuiver and Braziunas* [1989, 1993] used the ^{14}C content of tree rings as a proxy for solar variability. ^{14}C production in the atmosphere is modulated by the cosmic ray flux, which in turn is controlled by solar activity. By measuring the ^{14}C content of a tree ring of known age, accounting for influences by the Earth's geomagnetic field, and modeling climatic influences on ^{14}C production, the residual signal can be attributed to solar variability. Jürg Beer has used the ice core record of ^{10}Be to reconstruct solar variability [*Beer et al.*, 1988, 1990, 1994a, 1994b] on timescales of hundreds to thousands of years. ^{10}Be is produced by spallation reactions with nitrogen and oxygen in the upper atmosphere; during periods of higher solar activity, high-density magnetic regions in the solar wind can inhibit the production of ^{10}Be in the atmosphere, resulting in an inverse relationship between ^{10}Be concentration and solar radiative flux. Beer has been able to document the 11-year sunspot cycle in the ^{10}Be record.

The reconstruction of solar irradiance that we present here [*Rind et al.*, 1999] is extended from *Lean et al.* [1995] by using ^{10}Be ice core and ^{14}C tree ring data to estimate solar irradiance for 1500-1609. The post-1610 record [*Lean et al.*, 1995] was created by coupling the 11-year Schwabe cycle with a lower-frequency background component. The higher-frequency Schwabe-cycle record was constructed from direct observations of sunspot number as well as measurements of sunspot darkening from the Greenwich Observatory (after 1874). The lower-frequency component was derived from calibration with emissions from sunlike stars, scaled to result in an increase in total solar irradiation of 0.19% from the maunder minimum to the present.

A spectrally integrated solar irradiance reconstruction for the period 1500 to the present (Figure 3) clearly shows the Spörer minimum in the 1500s, followed by the well-known maunder minimum (1645-1715). Following a nineteenth century minimum (the Dalton minimum), a generally increasing trend in irradiance is seen for the twentieth century. Prior to 1720 the solar irradiance reconstruction may be missing a higher-frequency component (~11 year period) due to a lack of data that can be used to constrain the variability. Comparison among the reconstruction of solar irradiance and the ^{10}Be ice core and the ^{14}C tree ring data from *Beer et al.* [1990] and *Stuiver and Braziunas* [1993] (Figure 3) shows a general confirmation of the time-dependent shape of total solar irradiance. The primary disparity between the solar irradiance and the ^{10}Be data sets is related to the fact that the minima in the sunspot number are always close to zero and therefore show little variation, whereas the corresponding ^{10}Be maxima vary significantly; this indicates that sunspots and ^{10}Be are not thought to be identical indicators of overall solar variability, especially at periods of sunspot minima. The concentration of ^{10}Be depends not only on the production rate but also on several shorter-scale atmospheric processes, such as latitudinal mixing, exchange through the tropopause, and precipitation from the troposphere. Discrepancy between the amplitudes of the variability of the two data sets can therefore be explained by the 1- to 2-year residence time of

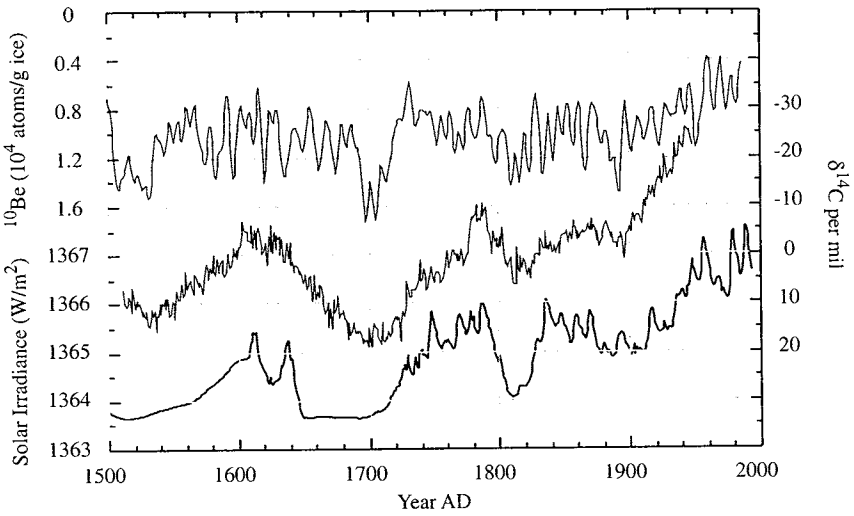

Figure 3. Reconstructed solar irradiance (bottom line, lower-left *y* axis) for the period 1500 to the present [*Rind et al.*, 1999] based on the sunspot record of solar activity, calibrated with emissions from sunlike stars. Clearly shown is the maunder minimum (1645-1715) as well as a generally increasing trend in irradiance for the period from 1900, following a nineteenth century minimum (the Dalton minimum). The ice core record of ^{10}Be (middle line, right *y* axis) from *Beer et al.* [1990] and the tree-ring record of ^{14}C (top line; top-left *y* axis) from *Stuiver and Braziunas* [1993] are inversely proportional to the record of solar irradiance (note reversed *y* axes). The annually resolved solar reconstruction is available at http://www.ngdc.noaa.gov/paleo/.

^{10}Be in the atmosphere as well as tropospheric production of ^{10}Be, which is not modulated by solar activity. The ^{14}C record (Figure 3) can be used to isolate the higher-frequency climate-induced variability seen in the ^{10}Be record. The ^{14}C record confirms the lower-frequency time-dependent patterns of change in the solar irradiance reconstruction; after 1850, however, the Suess effect forces the ^{14}C record to more depleted values, due to the injection of dead carbon into the atmosphere through fossil fuel combustion.

2.4. Volcanic Aerosols (1500 to Present)

Highly explosive volcanic eruptions can inject water vapor (H_2O), carbon dioxide (CO_2), sulfur dioxide (SO_2), chlorine (Cl^-), fluorine (F^-), and ash (particulate rock and pumice) into the stratosphere. The resultant HCl and HF is very soluble in water and falls to the ground as acid rain but can be ascribed onto ash particles within the eruption plume, also settling out quickly [*Rose*, 1977]. However, most of the SO_2 is quickly (~1 month) converted to sulfuric acid (H_2SO_4), which in turn condenses into fine droplets (aerosols). These sulfate aerosols reflect radiation from the Sun thus cooling the troposphere; sulfate aerosols can also absorb both infrared (terrestrial) radiation and insolation, warming the stratosphere. Sulfate aerosols also promote ozone destruction by altering chlorine and nitrogen chemical species in the stratosphere [*Cadle et al.*, 1976; *Hofman*, 1987; *Pollack et al.*, 1993; *Sato et al.*, 1993; *Schimel et al.*, 1996; *Solomon et al.* 1998]. Finally, incursion of stratospheric aerosols into the upper troposphere may have an indirect effect on climate by acting as cloud condensation nuclei for high clouds [*Schimel et al.*, 1996; *Sigurdsson*, 1990], although this effect is poorly understood at this time. Excellent summaries of the relationships between explosive eruptions and climate can be found in *Robock* [2000] and *Zielinski* [2000].

2.4.1. Volcanic indices. There have been multiple efforts to compile a quantitative record of the climatic effects of past volcanic eruptions. The earliest compilation (dust veil index (DVI) [*Lamb*, 1970; 1977; 1983]) extends from 1500 to 1982 and is based primarily on historical accounts of optical phenomena such as dry fogs and red sunsets; surface radiation measurements were used when available. In a few cases, reports of cooling associated with volcanic aerosols were incorporated into the index [*Lamb*, 1970, 1977, 1983]. All values of the DVI were standardized to result in a global DVI of 1000 for the 1883 Krakatau eruption; then the DVI values are scaled so that 40% of the index occurs in the year of the eruption, 30% in the year following the eruption, followed by 20% and 10% in years 3 and 4; latitudinally dependent estimates of the DVI have also been made [*Robock*, 1981]. The DVI is primarily a historical observational index and therefore most reliable for volcanic eruptions that affected populated areas within the last 300 years. *Lamb* [1970] also suggests that use of the DVI be limited to only an estimation of the order of magnitude of the atmospheric effect of a particular volcanic eruption. Finally, users of the DVI should be cautious of circular arguments when using DVI values derived from temperature data, though such estimates are clearly identified by *Lamb* [1970].

A second index that has received widespread attention is the volcanic explosivity index (VEI) [*Newhall and Self*, 1982], which uses geological evidence as a proxy for the measure of the power of the eruption. Eruptions dating back as far as 12,000 years ago have been assigned tentative VEI values; VEI values are still being assigned to eruptions that occur today [e.g., *Simkin and Siebert*, 1994]. The VEI can range from 0 to 8, with each interval representing a tenfold increase in explosivity; stratospheric injection is one of the criteria associated with eruptions with a VEI of 4 or higher but is considered one of the least reliable criteria [*Simkin and Siebert*, 1994]. For this reason, not all volcanic eruptions that have been assigned a VEI of 4 or higher have had a significant impact on the climate system. Also, as this index does not take into account the sulfur content of the gases

released, it cannot be directly used to estimate sulfate loading in the stratosphere. However, the VEI can be helpful in associating volcanic eruptions from the historical record with sulfate peaks found in ice core data.

More recently, *Sato et al.* [1993] produced a zonally averaged compilation of optical depth for volcanic eruptions stretching back to 1850. This data set is historical for the most part, with observational sources similar to the DVI in addition to land-based pyrheliometric measurement of atmospheric extinction for the period after 1882. Since 1979, satellite measurements have been made using the Stratospheric Aerosol Monitor (SAM) II and the Stratospheric Aerosol and Gas Experiment (SAGE) I and II instruments for polar and low-latitude regions, respectively [*Sato et al.*, 1993]. Most recently, *Stothers* [1996] has improved upon the *Sato et al.* [1993] reconstruction for the period 1881-1960 by incorporating more pyrheliometric data from stations primarily in the Northern Hemisphere. *Stothers* [1996] also used historical accounts of starlight extinction, purple twilight glows, and other turbidity indicators to support and expand upon the pyrheliometric data.

Ice cores offer a valuable opportunity to reconstruct volcanic aerosols through the measurement of volcanic sulfate (SO_4^{2-}) deposited on glacial ice in the years immediately following an eruption. The high temporal resolution (annual to biennial), the length of the records, and the low temporal error (e.g., $\pm$ 2 years for uppermost part of the Greenland Ice Sheet Project Two (GISP2) core [*Zielinski,* 1995]) available in many ice core records allow for the reliable quantification of the atmospheric impact of past volcanism prior to the period of reliable historical observations. Numerous efforts have been made to use acidity data from ice cores as a proxy for the record of volcanic eruptions. *Hammer et al.* [1980] used this method to produce a 10,000-year record of volcanism using both the Crete and the Camp Century ice cores from Greenland. *Crowley et al.* [1993] reanalyzed the Crete ice core record to quantify more precisely nonvolcanic values of sulfate and constructed a 1420-year record of volcanic activity. The GISP2 ice core has been used to create a 2100-year record of stratospheric loading and optical depth estimates and a 110,000-year record of explosive volcanism [*Zielinski*, 1995, 1996]. Finally, *Robock and Free* [1995, 1996] pioneered the use of sulfate data from multiple ice cores to construct a record of volcanic activity. They calculated an ice core-volcano index (IVI) for both the Northern Hemisphere and the Southern Hemisphere, derived from multiple data sets from Greenland, Mount Logan, Peru, and Antarctica, extending back to 1400 A.D. The IVI correlates well with the VEI and optical depths from *Sato et al.* [1993]; it correlates to a lesser extent with the DVI [*Lamb,* 1970]. The IVI was used as input for a series of energy balance model simulations of climate for the past six centuries [*Crowley and Kim,* 1999; *Free and Robock,* 1999].

2.4.2. The new ice core volcanic index. There are three motivations for producing a new record of stratospheric optical depth: (1) our new volcanic index that we present here combines historical observations, ice core data from both Greenland and Antarctica, as well as recent satellite data; (2) we have incorporated ice core data that were unavailable for the previous reconstructions and avoided ice cores that are less well dated or strongly complicated by nonvolcanic aerosols; (3) our new reconstruction is latitude dependent, with a variable zonal band width that is appropriate for climate-modeling studies. Our new volcanic aerosol index will hereafter be simply referred to as the VAI, a high-resolution time and latitude-dependent estimate of stratospheric optical depth for the past 500 years.

As summarized below and described in more detail following the summary, a multistep process was used to develop the VAI, starting with raw ice core sulfate data.

1. Biannually sampled GISP2 data were converted into estimated annually resolved values (all other ice core data were initially sampled at an annual resolution).
2. Potential volcanic peaks in the sulfate data were highlighted; the source volcano was identified, where possible, using historical records.
3. Recent increasing levels of anthropogenic sulfate were removed from the raw sulfate data by subtracting a low-frequency background trend.
4. Two average time series (one from Greenland ice core data and one from Antarctica ice core data) of sulfate flux were calculated from the detrended data.
5. Two local optical depths (at the latitude of the ice cores) were calculated for each year of the record.
6. For years with either no sulfate peak or no matching source volcano (from step 2), a linear latitudinal trend was established between the points calculated in step 5.
7. For years with a sulfate peak and matching source volcano (from step 2), a nonlinear trend was established between the points calculated in step 5, with the highest optical depths at the latitude of the eruption.

Excess sulfate (SO_4^{2-}) flux ($kg/km^2/yr^1$) data from five ice cores (GISP2, GR89, and Site A in Greenland; Siple and Dyer Plateau in Antarctica; Table 3, Figure 4) were provided by *Zielinski* [1995] (GISP2), *Cole-Dai et al.* [1995] (Dyer Plateau), and *Mosley-Thompson et al.* [1993] (all other cores). These cores were selected because they provide high

Table 3. Description of Ice Cores Used to Create the Ice Core Volcanic Index

Ice Core	Latitude	Longitude	Elevation (m asl)	Years of Record Used	Reference
Dyer Plateau	70° 40' S	64° 52' W	2002	1505-1989	*Cole-Dai et al.* [1995]
GISP2	72° 35' N	38° 28' W	3210	1500-1985	*Zielinski* [1995]
GR 89	72° 35' N	38° 27' W	~3200	1731-1989	*Mosley-Thompson et al.* [1993]
Siple	75° 55' S	84° 15' W	1054	1500-1983	*Mosley-Thompson et al.* [1993]
Site A	70° 38' N	35° 49' W	3090	1715-1985	*Mosley-Thompson et al.* [1993]

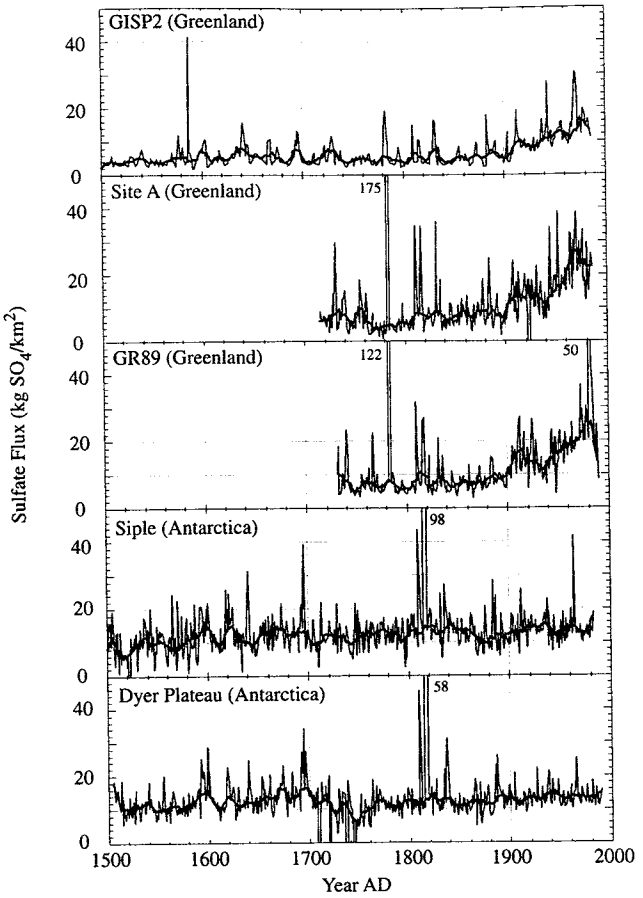

Figure 4. Time series of excess sulfate flux from GISP2 [*Zielinski*, 1995], Site A [*Mosley-Thompson et al.*, 1993], GR89 [*Mosley-Thompson et al.*, 1993], Siple [*Mosley-Thompson et al.*, 1993], and Dyer Plateau [*Cole-Dai et al.*, 1995] ice cores that were used to reconstruct the volcanic optical depth record for 1500 A.D. to the present. An 11-year running mean of each time series with the major volcanic peaks removed (bold line) was used to remove the low-frequency background sulfate in all five ice cores; the anomalous data in the Dyer Plateau data between 1700 and 1760 were not used. Numbers within the graphs show the maximum height of flux values extending above the range of the *y* axis. Ice core data are available at http://www.ngdc.noaa.gov/paleo/.

resolution, well-dated records of volcanic sulfate which were available in the public domain (http://www.ngdc.noaa.gov/paleo). Low-latitude, high-elevation ice core records were not used because of the heavy influence of nonvolcanic aerosols (e.g., sulfate from local desert sources) in these cores. All data except for that from GISP2 had been corrected for the presence of sea-salt sulfate [*Mosley-Thompson et al.*, 1993; *Cole-Dai et al.*, 1995], the primary nonvolcanic component of naturally derived sulfate in the high-latitude ice cores. *Zielinski* [1995] did not correct for sea-salt sulfate in the GISP2 data but estimated the sea-salt-induced error to be less than 5%. Finally, all data except for those from GISP2 were annually resolved; the GISP2 data were sampled continuously at an approximate biannual resolution. To make the GISP2 data compatible with the rest of the ice core data, biannual data were binned into annual increments based on the proportion of the sample from each individual calendar year (step 1 above).

The raw sulfate flux data from each of the Greenland ice cores show a recent background trend that was hypothesized to be the result of tropospheric anthropogenic sulfate deposition (Figure 4). This trend was removed following methodology modified from *Robock and Free* [1995]: first we calculated the standard deviation for each time series. We then identified any potential volcanic peaks (step 2 above) by selecting each peak that was larger than the average of the previous three years by twice the standard deviation; if one of the previous three years had been identified as a potential volcanic peak, the three previous nonvolcanic years were chosen for comparison. The identified volcanic peaks were then set equal to the mean of the remaining data. The entire procedure was then repeated as the initial standard deviation calculation included the largest volcanic peaks which were removed in the first round. An 11-year running mean was then calculated for this modified data set; this was considered to be the background volcanic signal (thick line in Figure 4). This elaborate peak identification process was used so that the 11-year running mean would approximate the low-frequency

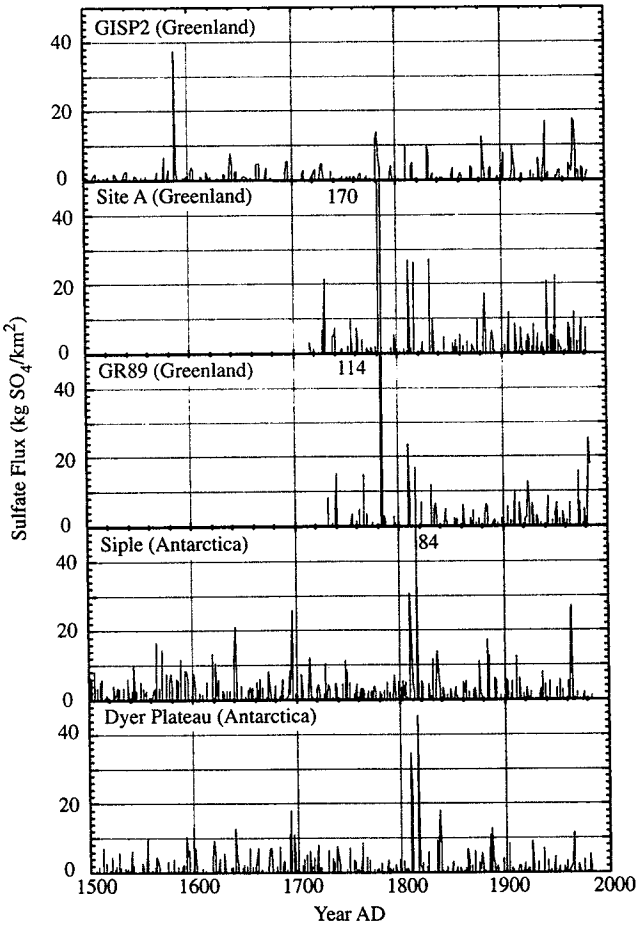

Figure 5. Time series of excess sulfate from GISP2 [*Zielinski*, 1995], Site A [*Mosley-Thompson et al.*, 1993], GR89 [*Mosley-Thompson et al.*, 1993], Siple [*Mosley-Thompson et al.*, 1993], and Dyer Plateau [*Cole-Dai et al.*, 1995] ice cores with the low-frequency background sulfate removed. Residual peaks shown here were calculated by subtracting the low-frequency background sulfate (as shown in Figure 4) from the raw data. Numbers within the graphs show the maximum height of flux values extending above the range of the *y* axis.

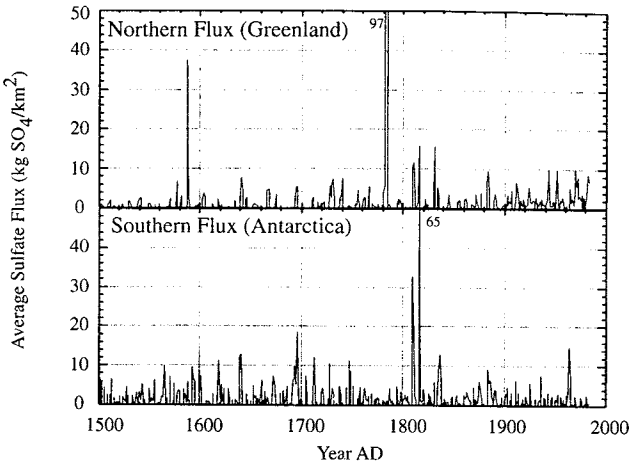

Figure 6. Detrended excess sulfate data from each of the ice cores were averaged in an effort to remove any biases associated with individual ice cores; an average annual sulfate flux time series is shown from both the Greenland ice cores and the Antarctica ice cores.

background variability in the time series and not be distorted by extreme sulfate peaks resultant of major volcanic eruptions. Finally, the background volcanic signal was subtracted from the raw data to create a detrended time series of sulfate flux (Figure 5 (step 3 above)). The above procedure was applied to both the Greenland and the Antarctica ice core data.

In an effort to remove any bias associated with individual ice cores, an average sulfate flux time series was calculated for both Greenland (i.e., average of three cores) and Antarctica (i.e., average of two cores), as shown in Figure 6 (step 4 above). The effect of this is to smooth out any localized effects that are not indicative of the true sulfate deposition, as can happen due to wind scouring. This averaging may also result in a lower maximum estimate of the stratospheric loading for each eruption by spreading the loading over a slightly longer period of time; the effects of this will be discussed below.

The next step in calculating the latitudinal profile of volcanic optical depth was to calculate the local optical depth perturbation (τ) at the latitude of the ice cores for each year of the record (step 5 above). This was defined by *Stothers* [1984] to be

$$\tau = \sigma n l, \tag{1}$$

where

$$\sigma = \pi r^2 Q, \tag{2}$$

$$n = \frac{M}{Alm}, \tag{3}$$

and

$$m = \frac{4\pi r^3 \rho}{3}, \tag{4}$$

where σ is the mean scattering coefficient, n is the number density of the aerosols, l is the vertical path length through the aerosol layer, r is the mean aerosol radius, Q is a dimensionless scattering factor, M is the sulfate loading over an area A, and ρ is the mean aerosol density. Incorporation of characteristic values of r, Q, and ρ of 0.3 μm, 2, and 1.5 g/cm^3, respectively [*Stothers*, 1984], results in the annually averaged τ at the latitude of the ice cores (70°-75° N/S) being equivalent to the non-sea-salt ice core sulfate flux (M) in g/m^2 multiplied by a coefficient of 3.33 m^2/g.

For years with no sulfate peak identified as above (following the methodology developed by *Robock and Free* [1995]), a latitudinal profile was estimated as a linear trend in optical depth between the two latitudes of the ice cores (step 6 above). This matches up well with modern satellite and instrumental data which suggests that the latitudinal profile is nonlinear during the year of a major eruption but can be approximated linearly for noneruption years, including those years immediately following an eruption [*Sato et al.*, 1993]. If a sulfate peak, identified using the methodology of *Robock and Free* [1995] described above, could not be associated with a known historical eruption, a linear trend was established as well, because no other tie points were available to constrain a nonlinear latitudinal profile.

However, if a volcanic peak in the ice core sulfate record could be matched up with a known eruption in the historical record, a nonlinear latitudinal profile was developed (step 7 above). Analysis of annually averaged stratospheric optical depth data from *Sato et al.* [1993] of three recent years with major eruptions (Agung, 1963, VEI=4; El Chichón, 1982, VEI=5; and Pinatubo, 1991, VEI=6) shows a general pattern of elevated optical depth approximately centered over the latitude of the eruption, with an approximately linear trend of background optical depths on either side (poleward) of this peak (Figure 7a). This pattern is not so evident in the southern extent of the 1963 Agung plume, perhaps due to a lack of data in the high southern latitudes, resulting in interpolation between the few available data points (Figure 7a), suggesting that the latitudinal width of the annually averaged Agung eruption plume is a maximum estimate. A simple linear relationship was established between time of year of the eruption and the width (in degrees of latitude) of the peak of elevated optical depth (Figure 7b); a hypothetical December 31 eruption is also included to constrain further the linear relationship. While results from so few data points cannot identify a statistically significant relationship between the time of year of an eruption and the annually averaged poleward extent of the eruption plume, and also ignore such nonquantifiable effects such as the quasi-biennial oscillation, we do suggest here that an eruption occurring earlier in the year allows for farther poleward transport of the eruption plume over the course of the year. It is important to note that any error incorporated here will only be related to the latitudinal width of the peak of elevated optical depth: as will be described below, this part of the methodology in no way affects the globally averaged optical depth.

We used the least squares linear relationship from these data to estimate the width of the elevated optical depth peak in our reconstructed annually averaged latitudinal profile of stratospheric optical depth for each year in the record with an identified volcanic eruption. Poleward of this peak, a linear trend was maintained (as was used for the entire latitudinal profile of noneruption years). It is worth noting from Figure 7a that the annually averaged distributions for El Chichón and Pinatubo are quite different, even though the eruptions were only separated by 2° of latitude, showing the importance of the prevailing stratospheric circulation on the aerosol distribution, a factor that we cannot account for in our reconstruction. Finally, it is worth noting that each of the three eruptions that we used to characterize the stratospheric

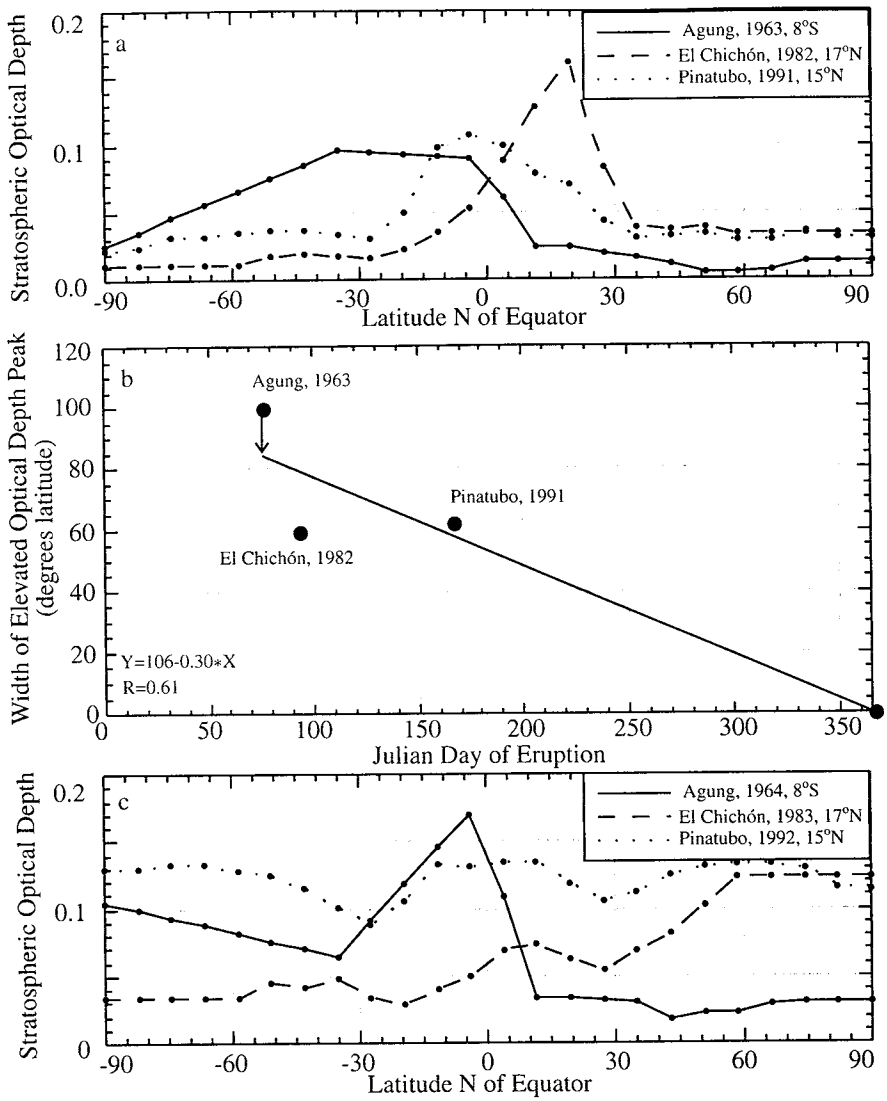

Figure 7. Annually averaged stratospheric optical depth data from *Sato et al.* [1993] of three recent years with major eruptions (A, Agung, 1963; El Chichón, 1982; and Mount Pinatubo, 1991) suggest a simple relationship between time of year of the eruptions and the width (in degrees of latitude) of a peak of elevated optical depth centered over the latitude of the eruption. A hypothetical December 31 eruption is included in Figure 7b to further constrain the linear relationship; the latitudinal width of the 1963 Agung plume is considered a maximum estimate due to interpolation between sparse data points. Except for the latitudinal profile in 1964 (the persistence of an optical depth peak is due to the extended nature of the Agung eruption), plot C shows that the latitudinal profile for the year following each eruption may be approximated as a simple linear trend. See text for details.

transport volcanic plumes were equatorial eruptions. The VAI could be improved substantially by the incorporation of data from higher-latitude eruptions, however there have been no highly explosive high-latitude eruptions during the period of record of satellite data.

We use the latitudinal profiles shown in Figure 7c as evidence for the pattern of the latitudinal distribution of optical depth in the year following a particular eruption. Both 1983 and 1992 (the years following the eruptions of El Chichón and Pinatubo, respectively) suggest that the latitudinal distribution of optical depth can be best represented as a linear trend of globally elevated optical depth. Year 1964 (following Agung) presents a more complicated scenario due to the temporal persistence of the eruption: Agung continued to be active until January 1964 [*Simkin and Siebert*, 1993]. It remains curious, however, as to why a distinct peak in optical depth remains in the annually averaged latitudinal profile for 1964. If this apparent peak is real and not an artifact of poor coverage in the presatellite era, it highlights one limitation of our method; a summary of such limitations will be described in further detail below. Despite the complications related to the eruption of Agung, we chose to represent all latitudinal profiles in each of the years immediately following an identified eruption as a linear trend, with two tie points being the calculated optical depths at the latitudes of each of the ice cores. In summary, the data from *Sato et al.* [1993] suggest that the latitudinal profile of annually averaged optical depth for the year of a highly explosive eruption can be generally

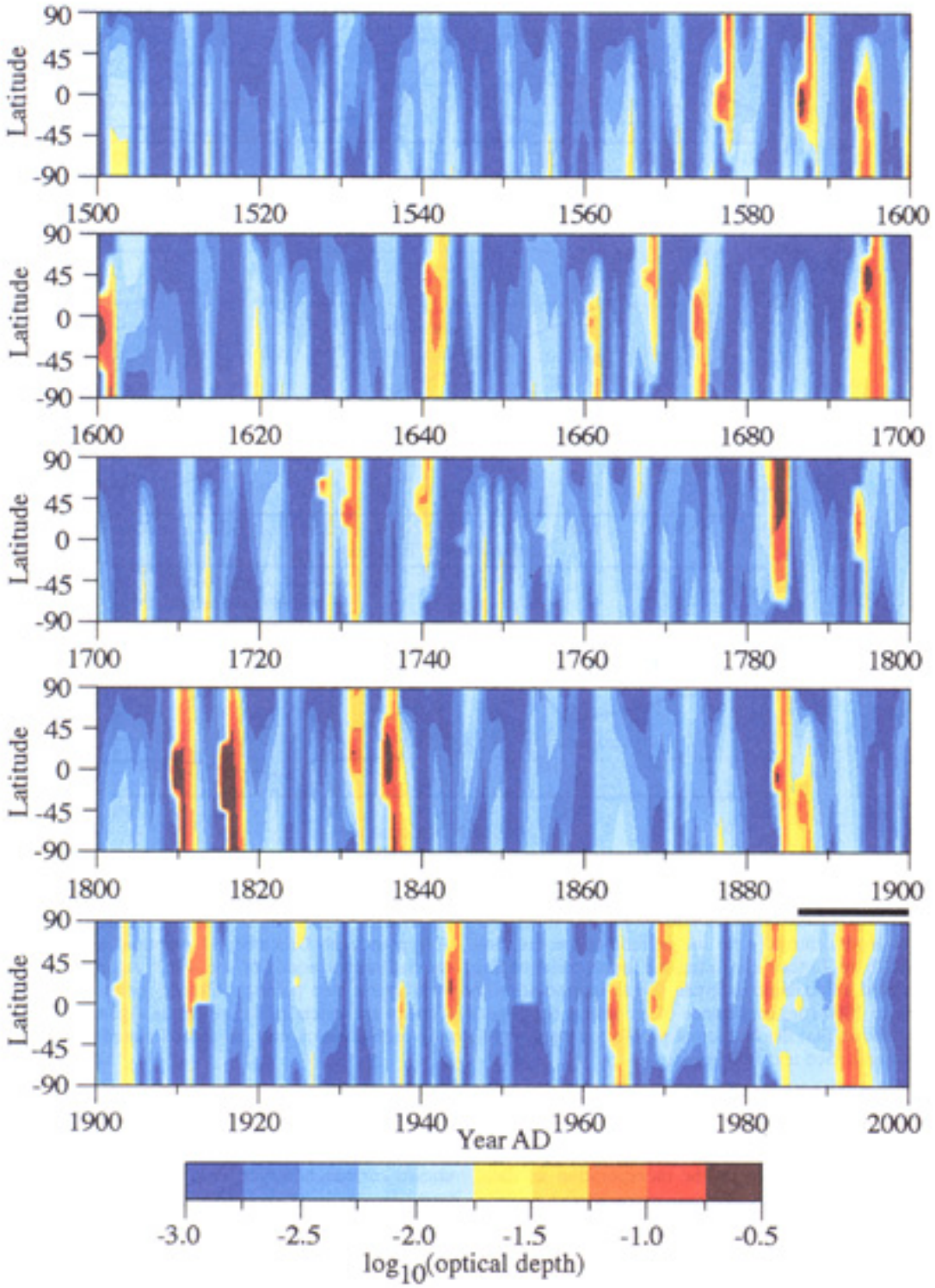

Plate 3. VAI is a reconstruction of annually resolved, zonally averaged stratospheric optical depth as a function of explosive volcanic activity for the period 1500-1983. As indicated by the horizontal black line, data shown here for the period 1984-1999 are from *Sato et al.* [1993]. The gridded global array of estimated annually resolved volcanic optical depth is available at http://www.ngdc.noaa.gov/paleo/.

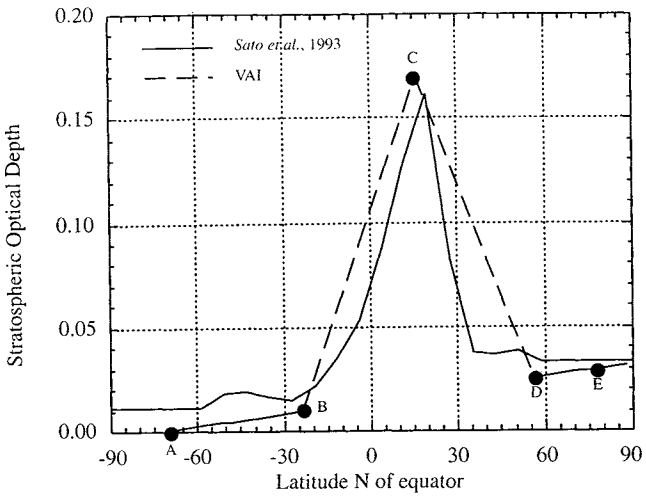

Figure 8. Latitudinal profile of stratospheric optical depth for 1982, the only year in which satellite data and the VAI overlap; 1982 was dominated by the April 3 eruption of El Chichón, in southern Mexico. Points A and E on the VAI plot were determined from the average latitude of the ice cores and the local optical depth calculated using formulae from *Stothers* [1984]. The latitude of points B and D were calculated using the least squares relationship from Figure 7b: the time of year of the eruption determines the width of the peak of elevated optical depth; the optical depths at points B and D are based on a linear trend established between points A and E. Finally, the latitude of point C is based on the latitude of the volcano; the optical depth at point C is adjusted until the integrated global optical depth was equal to the independently derived global optical depth calculated using methodology developed by *Zielinski* [1995] for the GISP2 ice core data (based on fallout rates of bomb nuclides developed by *Clausen and Hammer* [1988] and scattering formulae developed by *Stothers* [1984]).

characterized by a narrow zone of elevated optical depth, poleward of which lower optical depths are found. The year following the eruption can be generally characterized by a linear trend of elevated optical depths from pole to pole.

The next step in the calculation of the latitudinal profile for years with identifiable volcanic eruptions was to estimate the maximum optical depth at the latitude of the eruption. This maximum optical depth was calculated iteratively by adjusting its value until the integrated global optical depth in our reconstruction was equal to the independently derived global optical depth calculated using the methodology developed by *Zielinski* [1995] for the GISP2 ice core data based on transport ratios of bomb nuclides developed by *Clausen and Hammer* [1988] and scattering formulae developed by *Stothers* [1984]. As an example, Figure 8 shows the observed annually averaged latitudinal profile for 1982 [*Sato et al.*, 1993] in comparison with the annually averaged latitudinal profile from the VAI for 1982. Also highlighted in Figure 8 are the five points that we used to constrain this particular latitudinal profile.

The final step in the calculation of the VAI involved a correction in the optical depths for the year immediately following each eruption. Examination of the VAI without this correction (when compared with the DVI, *Sato et al.* [1993], and the analysis of the 1815 Tambora eruption by *Stothers* [1984]) showed that the VAI underestimated the stratospheric optical depth for the year immediately following each major eruption. The average northern and southern sulfate flux time series (Figure 6) were then examined to estimate how much of the total sulfate attributed to a particular eruption was deposited on the ice in the calendar year following each eruption. The linear latitudinal trend of stratospheric optical depth estimated for the year following each particular eruption was then uniformly elevated so that the calculated optical depth for that year relative to the calculated optical depth for the year of the eruption was equivalent to the ratio of ice core sulfate flux deposited after the year of the eruption relative to the total ice core sulfate flux attributed to that particular eruption.

Our new volcanic aerosol index (VAI) is a latitude- and time-dependent reconstruction of global stratospheric optical depth from highly explosive volcanic eruptions (Plate 3). The VAI

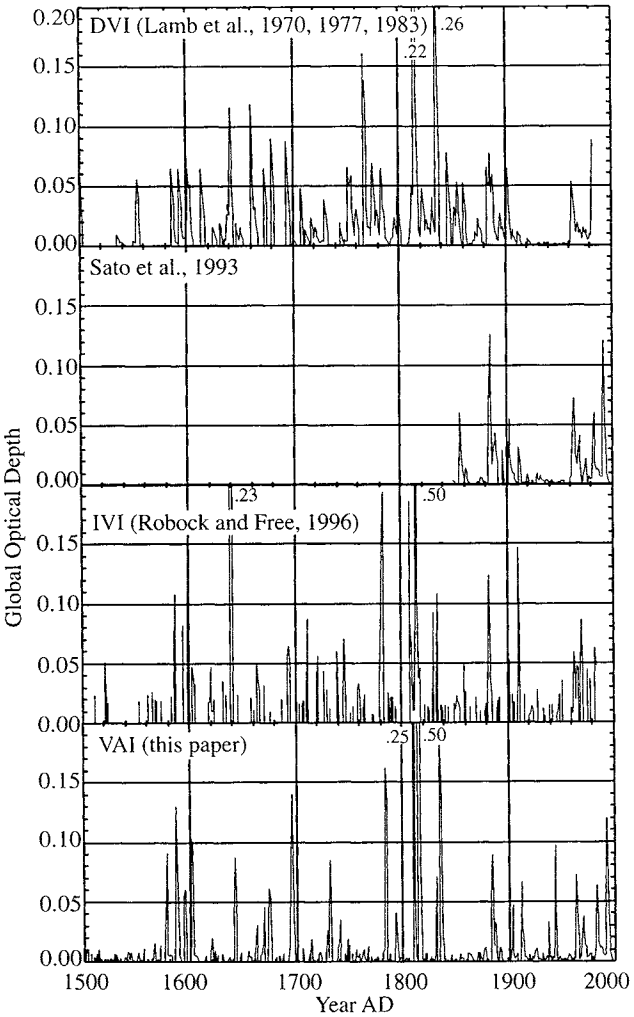

Figure 9. Comparison of time series of globally averaged volcanic indices: (a) dust veil index (DVI) [*Lamb*, 1970, 1977, 1983], (b) *Sato et al.* [1993], (c) ice core volcanic index (IVI) [*Robock and Free*, 1996], and e) VAI (this paper). The DVI (Figure 9a) is based on historical accounts of optical phenomena such as dry fogs and red sunsets caused by explosive volcanic eruptions which were then quantified and standardized so that the time-integrated DVI associated with the 1883 eruption of Krakatau was given a global value of 1000. For comparison purposes we calculated optical depths from the DVI by calibrating the DVI to our VAI optical depths for the Krakatau eruption.

shows elevated stratospheric optical depth from individual eruptions extending to the north and south for the year of the eruption, temporally restricted to the two years following the eruption. In general, the majority of the highly explosive eruptions that have occurred over the last 500 years are in either the Northern Hemisphere or slightly south of the equator.

2.4.3. Comparison with other volcanic indices. The VAI is the first latitude- and time-dependent continuous reconstruction of volcanic optical depth for the past 500 years. As seen in Figure 9, our index is similar in general to that presented by others but has some noticeable areas of disagreement, particularly in the period 1915 to 1960, but also in the preceding century. The following analysis will emphasize the period 1800 to the present, as that includes the interval over which all indices are most complete and reliable. However, we will also comment on comparisons between our new record, the DVI, and the IVI for the period 1500-1800, focusing only on the most significant eruptions. For comparison purposes, the DVI in Figure 9 was scaled to optical depth by calibrating to our calculated integrated VAI optical depth (0.16) for the years 1883-1885, the years influenced by the eruption of Krakatau (6°S, Indonesia).

1500-1800: The first major eruption noted in the VAI occurred in 1577, as evidenced from elevated levels of sulfate levels in both the Greenland and the Antarctica ice cores. We attributed this sulfate to the eruption of Billy Mitchell (6°S, Bougainville), based on the *Simkin and Siebert* [1993] date of 1580±20 years. *Zielinski* [1995] had assigned the 1588 sulfate peak in the GISP2 core to both Billy Mitchell and Kelut (8°S, Indonesia), but we attributed the entire 1588 sulfate loading to the better dated Kelut eruption and assigned the Billy Mitchell eruption to the 1577 sulfate, resulting in a peak global optical depth of 0.09 in 1577, in contrast to the value of 0.00 calculated by *Lamb* [1970]. Next, the calculated global optical depths from the VAI for the 1586 eruption of Kelut (0.13) is significantly larger than the DVI value of 0.06, and slightly larger than the IVI value of 0.11, in large part due to the extremely high sulfate loading in the GISP2 core, which exceeded even the GISP2 sulfate flux following the 1815 eruption of Tambora. Next, the VAI global optical depth of 0.06 following the 1593 eruption of Raung (8°S, Indonesia) matches up well with the DVI value of 0.07, and the IVI value of 0.08.

Comparison between the VAI and the DVI show good agreement on the 1600 eruption of Huaynaputina (17°S, Peru). The VAI has a global optical depth of 0.10, with higher loading in the Southern Hemisphere, due to the southern latitude of Huaynaputina; the IVI shows a similar globally averaged value of 0.14. Although the DVI did not identify the eruption, *Lamb* [1970] presented a calculated optical depth of 0.06, with the majority of the sulfate loading in the Northern Hemisphere. However, all three of these estimates are much lower than the estimate by *de Silva and Zielinski* [1998] which suggested that the atmospheric impact of the Huaynaputina eruption was up to 78% of the atmospheric impact of the 1815 Tambora eruption (which we calculated as having a maximum global optical depth of 0.5).

The VAI indicates that the eighteenth century was characterized by less stratospheric sulfate loading than indicated by both the DVI and the IVI, particularly in the period 1750 to 1780. One of the few significant events of the eighteenth century was the 1783 eruption of Laki (64°N, Iceland); estimates in the DVI have values of about 0.06; the VAI and the IVI show significantly higher global values of about 0.16 and 0.19, respectively.

The 1800s: The VAI suggests that the early part of the nineteenth century was characterized by the largest eruptions of the past 500 years, whereas the period 1836 to 1882 showed generally less loading than indicated by the DVI and *Sato et al.* [1993]. There is substantial ice core evidence of a major volcanic eruption occurring in 1809 [*Dai et al.*, 1991; *Moore et al.*, 1991]. When calculating the VAI, we placed the eruption at the equator, simply based on a high number of explosive volcanic eruptions that have occurred in the equatorial zone [*Simkin and Siebert,* 1993] and the high sulfate flux found in ice cores from both Antarctica and Greenland, however, we can not rule out the possibility of coincident middle- or high-latitude eruptions in each hemisphere. Our calculated global optical depth in the VAI is 0.25, comparable to the calculated optical depth of 0.19 in the IVI. *Lamb* [1970] did note some evidence of haze seen over London in early April 1809, as well as a sharp temperature decrease from 1807 to 1810, but refrained from calculating a DVI for 1809 due to the lack of a known volcanic eruption.

The eruption of Tambora (8°S, Indonesia) in 1815 was the largest volcanic eruption of the millennium (VEI=7 *Simkin and Siebert,* 1993), and resulted in the highest calculated global optical depth of the past 500 years, peaking with a value of 0.50 in 1815, precisely equal to the optical depth calculated in the IVI. *Stothers* [1984] calculated an even higher global optical depth of 0.85 in 1815, increasing to 0.9 in 1816 and then decreasing to 0.2 in 1817. In contrast to the estimates by *Stothers* [1984] the estimates by *Lamb* [1970] are much lower than those for the VAI. Calibrated global optical depths from the DVI peak at 0.22 in 1815 and then decline to 0.16, 0.12, and 0.06 in 1816, 1817, and 1818, respectively. Much of the discrepancy between the DVI and the VAI/IVI is seen in the Southern Hemisphere: the DVI estimated equal hemispherical loading; however, because of the higher sulfate flux values in the Southern Hemisphere ice cores, the calculated Southern Hemisphere optical depth (0.67) in the VAI is twice as large as the Northern Hemisphere optical depth (0.33) in 1815; the IVI similarly estimated higher Southern Hemisphere loading (0.72) compared to the Northern Hemisphere (0.27).

In 1831 the volcano Babuyan Claro (20°N, Philippines) erupted; *Lamb* [1970] estimated a global optical depth of 0.04 which he attributed to both Babuyan Claro and Campiflegrei Mar Sicilia (37°N, Italy). In the VAI we calculated a comparable global optical depth of 0.07, attributing all of the sulfate to the more explosive (VEI=4) Babuyan Claro eruption; the IVI shows a slightly higher optical depth of 0.09. This was followed by the 1835 eruption of Cosiguina (13°N, Nicaragua), which the DVI shows as resulting in the highest optical depths of the past 500 years (0.36), 20% higher than the calculated DVI global optical depth for the 1815 Tambora eruption. In contrast, a study by *Self et al.* [1989] suggests the atmospheric impact of Cosiguina to be minimal. The globally averaged VAI optical depth of 0.18 lies between these two extremes, suggesting that it was a major eruption, as coherent sulfate peaks were identified in each of the five ice cores but of significantly less impact than the Tambora eruption; the IVI shows an even lower optical depth of 0.11. The VAI shows very low optical depths between 1836 and 1883, as no major peaks were apparent in the ice core records,

though both *Sato et al.* [1993] and *Lamb* [1970] give high optical depths to the 1855-56 eruptions of Cotopaxi (1°S, Ecuador), with globally averaged optical depths of 0.05 and 0.06, respectively. However, as *Simkin and Siebert* [1993] assign this eruption a VEI of only 2, it was not considered in the calculation of the VAI. Finally, all indices agree fairly well with the VAI for the 1883 Krakatau eruption. The DVI from *Lamb* [1970] shows a peak global optical depth of 0.07, slightly lower than the VAI optical depth of 0.09 to which it was calibrated, because *Lamb* [1970] spread out the DVI optical depths over a longer period of time (4 years). The independently calculated optical depths from *Sato et al.* [1993] and from the IVI also agree in general with the VAI, yielding peak global optical depths of 0.13 and 0.12, respectively. In addition, the pyrheliometric estimates made by *Stothers* [1996] result in a peak mid-latitude optical depth of 0.14 in 1884, decreasing to 0.02 by 1886.

The 1900s: The new VAI suggests that the twentieth century was characterized by significantly more stratospheric sulfate loading than indicated by the DVI and *Sato et al.* [1993] in the period 1913 to 1962. All four indices agree fairly well with global optical depths following a series of 1902 eruptions, dominated by the eruption of Santa Maria (15°N, Guatemala) with a VEI of 6. Calculated optical depths were 0.06 by *Sato et al.* [1993] and *Lamb* [1970] and 0.05 in the VAI and in the IVI. Estimates from *Stothers* [1996] agree as well, with midlatitude Northern Hemisphere optical depths ranging from 0.05 to 0.10. Next, *Sato et al.* [1993] and *Lamb* [1970] both recognized the 1912 eruption of Novarupta (58°N, United States, formerly thought to be Katmai) but calculated relatively low optical depths of only 0.03 and 0.01, respectively. In contrast, the IVI shows globally averaged optical depths of 0.15, due to the high sulfate values in the Greenland and Alaskan ice cores. *Stothers* [1996] presents a range of pyrheliometric optical depth data for 1912-1914: latitudes north of 45° N showed an annual average optical depth of 0.24 in 1912, declining to 0.03 in 1914. Latitudes between 30° N and 45° N had an optical depth of 0.10 in 1912, declining to 0.03 in 1914. The VAI shows a peak globally averaged optical depth of 0.07, with a portion of the sulfate attributed to the 1911 equatorial eruption of Taal (14°N, Philippines), due to elevated levels of sulfate in 1911 in the Siple ice core.

The main period of discrepancy between historical (DVI *Stothers*, 1996; *Sato et al.*, 1993) and ice core records is the period 1913-1962, between the 1912 Novarupta and the 1963 Gunung Agung (8°S, Indonesia) eruptions. Both the DVI and the *Sato et al.* [1993] records show a continuously low baseline, with no stratospherically significant eruptions for the duration of this period; *Stothers* [1996] estimates optical depths less than 0.02 for the duration of the time period. Also, the IVI, shows a series of small eruptions, though none exceed 0.05 in global optical depth. The VAI, however, calculated significant optical depths in this time period based on three eruptions: Rabaul (4°S, Papua New Guinea) in 1937, Paricutin (19°N, Mexico) in 1943, and Lamington (9°S, Papua New Guinea) in 1951 eruptions, respectively. Part of the reason for the higher ice core derived optical depths may be contamination from anthropogenic aerosols due to tropospheric transport; however, distinct ice core sulfate peaks do tend to coincide with known explosive eruptions. In particular, much of the Southern Hemisphere ice core data, show significant sulfate peaks from 1915 to 1960, a period for which neither *Stothers* [1996], *Sato et al.* [1993], nor *Lamb* [1970] calculated significant optical depths. The 1937 eruption of Rabaul resulted in significant sulfate peaks in both Southern Hemisphere cores as well as a very small peak in the GISP2 record, resulting in a global optical depth of 0.03 in 1937. The high sulfate levels in the Southern Hemisphere ice cores suggest that the Northern Hemisphere based observational reconstructions were not able to pick up these major Southern Hemisphere dust veils. Next, all three Northern Hemisphere ice cores showed a major sulfate peak in either 1943 or 1944, which we attributed to the 1943 eruption of Paricutin (VEI=4; however, this particular value of the VEI may be mostly based on lava volume as opposed to stratospheric input), resulting in a calculated global optical depth of 0.10; no elevated sulfate levels were seen in the Southern Hemisphere ice cores. Despite the high sulfate levels in all the Northern Hemisphere ice cores, none of the historical records [*Sato et al.*, 1993; *Lamb,* 1970; and *Stothers*, 1996] identified any eruptions in the early and mid-1940s as being stratospherically significant. It thus appears that the period 1913-1963 may not have been as volcanically quiet as previously inferred.

As a result of the very high sulfate loading in both Antarctica ice cores in 1963-1964, we initially calculated an annually averaged global optical depth of 0.14 following the 1963 Gunung Agung eruption. This estimate significantly exceeded previous estimates: 0.05 in the DVI, 0.07 in the work of *Sato et al.* [1993], and 0.09 in the IVI. This estimate was also significantly higher than the satellite-measured optical depth for the 1982 El Chichón eruption (0.06, an eruption of comparable magnitude) and slightly higher than the satellite measured optical depth for the 1991 Pinatubo eruption (0.12, a significantly larger eruption). Because of this apparent inconsistency, we calibrated our ice core estimates with the global estimates by *Sato et al.* [1993] and new estimates from *Keen* [1997] based on visual extinction data from lunar eclipses, resulting in a revised global optical depth estimate of 0.07 for the Agung eruption. The remaining sulfate in the Antarctic may be indicative of either a local Antarctic eruption that cannot be accounted for in the historical record or shortcomings with the methodology that we used in calculating the VAI.

Finally, the VAI-calculated optical depth of 0.06 for the 1982 El Chichón (17°N, Mexico) eruption matches up well with the most accurate of all the records for this time period – the satellite derived optical depths of 0.06 in the Sato record (Figure 8) as well as the minimum estimate of 0.06 made by *Zielinski et al.* [1997] and the estimate of 0.06 in the IVI; the estimate from the DVI is slightly higher, at 0.12. Plate 3 and Figure 9 also include satellite data from *Sato et al.* [1993] for the period 1984-1999, the interval for which available ice core data is not complete. The 1991 eruption of Pinatubo (15°N; Philippines) results in a peak annually averaged global optical depth of 0.12 in 1992.

2.4.4. Limitations of the VAI. Despite the many advantages that ice cores offer in estimating past variability of stratospheric aerosols, there are some limitations associated with our method. First, all ice cores except the GISP2 core were sampled at annual resolution; the GISP2 core, however, was sampled in continuous 2-year segments, effectively smoothing the record. Because of this, the analysis of multiple eruptions occurring within a 2-year period becomes difficult. However, the use of annually resolved data

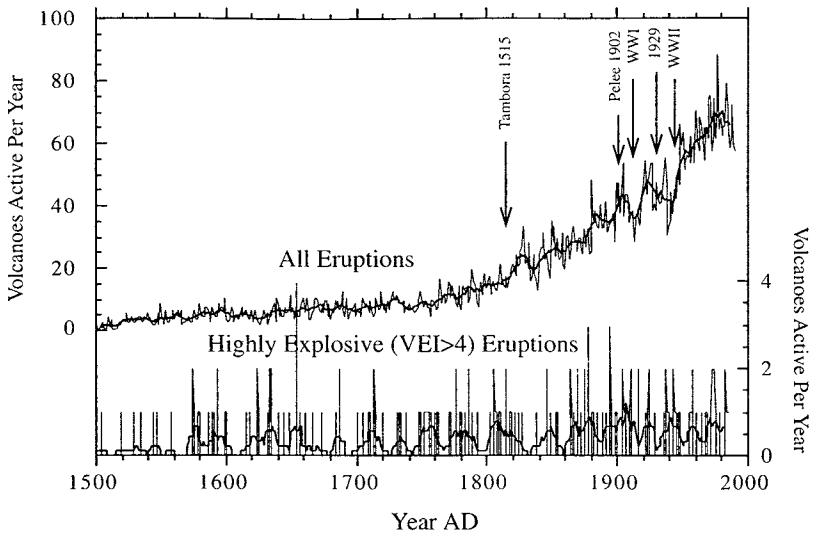

Figure 10. Frequency of volcanic eruptions reported per year for the last 500 years (modified from *Simkin and Siebert* [1993]). The top plot shows total number of volcanic eruptions reported per year with the 9-year running mean. The bottom plot shows only highly explosive (VEI $\geq$ 4) volcanic eruptions with the 9-year running mean.

from two additional ice cores (GR89 and Site A) helped eliminate these problems. Secondly, there are probable limitations to the historical record as well; however, these errors are probably limited to the earlier portion of the record (pre-1600). An eruption frequency plot (Figure 10; modified from *Simkin and Siebert* [1993]) suggests that the total number of volcanic eruptions reported per year is related to historical events (e.g., wars) and the number of potential observers (i.e., population). However, the frequency of highly explosive (VEI $\geq$ 4) eruptions shows no comparable trend (bias) for the last 400 years. The sixteenth century, however, shows significantly fewer highly explosive eruptions per year than the succeeding centuries. This is evidence for why both the VAI and the DVI identify fewer volcanic eruptions prior to 1575 (Figure 9). Fortunately, although in the calculation of the VAI the lack of historically documented eruptions does not allow for the calculation of a peak optical depth at the latitude of the volcano, this does not change the globally averaged optical depth. Although more infrequent, there are likely limitations to the historical record of volcanic eruptions after 1600. For example, as mentioned above, a major sulfate peak is seen in all six ice core time series in 1809, yet there is no corresponding eruption in the historical record (due to the coherent signal in each of the ice cores, this eruption was included in the VAI). Other more significant errors may exist in the rest of the historical record. A third limitation of the VAI involves ice core contamination by tropospheric aerosols. Although we were able to correct for the presence of anthropogenic sulfate in the ice core data, there are possible additional inputs of natural tropospheric sulfate aerosols. For instance, the most important volcanic event of the eighteenth century was the eruption of Laki in 1783. This eruption did penetrate the stratosphere [*Thordarson and Self*, 1993; *Fiacco et al.*, 1994] and lasted for over a year, continuously emitting sulfur, resulting in a persistent dry fog over Europe [*Franklin*, 1784]. Because of the proximity of the volcano and the persistence of the eruption, much of the sulfur emitted by Laki may have been transported to the ice through the troposphere. Fourthly, the model we used in estimating stratospheric transport is based on sparse data from atmospheric bomb testing [*Clausen and Hammer*, 1988], based on the assumption that volcanic aerosols will behave similarly to bomb fallout when injected into the stratosphere. This is, of course, strongly dependent on the phase of the quasi-biennial oscillation following the volcanic eruption. Also, our estimate of poleward transport over the course of the year of the eruption is based on analysis of a limited number of closely spaced (all were within 15° of the equator) eruptions; one of these eruptions (Agung) occurred prior to the period of satellite observations, increasing the uncertainty associated with the latitudinal profile of its associated optical depth. A fifth potential limitation to the VAI is the possibility of a sulfate signal from a major volcanic eruption not appearing in an ice core, as may be the case with sulfate from the Mount Pinatubo eruption not appearing in Greenland snow pits [*Zielinski*, 2000]. Hopefully, the use of multiple ice cores has kept this type of error to a minimum. Finally, we are unable to correct for the potential of local volcanic input to Antarctic ice cores, which may inflate the sulfate flux levels in a way that the historical record cannot correct for.

In summary, our new VAI can still benefit from the use of additional ice core and snow pit data as well as a more sophisticated analysis of stratospheric transport. However, it does represent a substantial improvement over previous attempts to reconstruct stratospheric volcanic aerosol loading for the last 500 years as it is the first reconstruction that combines ice core data and historical observations and uses the recent record of satellite data to produce a continuous high-resolution spatial and temporal record of the atmospheric effects of explosive volcanism since 1500 A.D. Also, our new index has been developed in a format that makes it appropriate both for modeling studies and comparison with paleoclimate proxy reconstructions.

3. Conclusions

We have compiled the first comprehensive database of climate forcing data specifically designed for climate

modeling studies for the period 1500 to 1999. Trace gas concentrations from fossil air trapped in glacial ice were used in conjunction with direct instrumental trace gas mixing ratio measurements that have been made since 1957 at various stations around the world [*Dlugokencky et al.*, 1994; *Keeling and Whorf*, 1994; *Prinn et al.*, 1994]. The Antarctic Law Dome ice core was used [*Etheridge et al.*, 1996] to produce a high-resolution CO_2 record for the period 1500 to 1969, which compares well during the period of overlap with the instrumental CO_2 data from Mauna Loa (Figure 1a). The Antarctic Mizuho ice core was used in conjunction with the Greenland Site J ice core [*Nakazawa et al.*, 1993] to produce a high-resolution CH_4 record for the period 1500 to 1951; instrumental CH_4 data are available from 1984. Finally, the Antarctic Byrd Station [*Khalil and Rasmussen*, 1988], Law Dome [*Etheridge et al.*, 1988], and Adelie Land [*Zardini et al.*, 1989] ice cores were all used to produce a high resolution N_2O record for the period 1500 to 1966; instrumental N_2O data are available from 1984 [*Prinn et al.*, 1994].

A time-varying global tropospheric aerosol optical depth distribution was created by scaling the modern distribution of tropospheric aerosol optical depth back to 1860 using regional CO_2 emission estimates. Modern anthropogenic aerosol optical depth estimates are a function of aerosols derived from both fossil fuel combustion and biomass burning; natural aerosols are a function of mineral dust transport and biogenic sulfate. Exponential curves fit to CO_2 emissions data for nine different regions of the world [*Marland et al.*, 1994, Figure 2] were then used as a proxy for anthropogenic aerosol emissions over time. Time-dependent CO_2 emission ratios relative to 1992 were then calculated for each region; these ratios were then used to standardize the modern model-derived optical depth distributions to 1992 values and to scale these values downward for past years; the natural aerosols were kept constant over the course of the reconstruction.

An improved reconstruction of solar irradiance has been presented, using the sunspot record of solar activity, calibrated with emissions from sunlike stars. Our spectrally integrated solar irradiance reconstruction for the period 1500 to the present clearly shows the maunder minimum (1645-1715) as well as a generally increasing trend in irradiance for the period from 1900, following a nineteenth century minimum (the Spörer minimum).

Finally, a new continuous, annually resolved volcanic aerosol optical depth time series has been created. The VAI combines historical observations, ice core data from both Greenland and Antarctica, as well as recent satellite observations; we have also incorporated ice core data that were unavailable for the previous reconstructions. The VAI is latitude dependent, with a variable zonal band width that is appropriate for climate-modeling studies. The VAI is an improvement over previous historical and ice core based reconstructions for all latitudes for the period from 1500 to 1900 and for the more sparsely populated Southern Hemisphere for the period 1900 to 1960.

Future studies would do well to reconstruct and test land cover change, mineral aerosols, and other hypothesized climate forcings on a high resolution spatial and temporal scale. All climate forcings shown here are currently being used as input to the NASA-GISS climate models for paleoclimate modeling experiments covering the period 1500 to the present.

Acknowledgments. We thank C. Amman, R. Bradley, and R. Stothers for valuable discussions related to our work; we also thank three anonymous reviewers for valuable feedback. Funding was provided by the United States National Science Foundation, National Oceanic and Atmospheric Administration, and National Aeronautics and Space Administration. Data were kindly provided by David Etheridge, Jürg Beer, the National Oceanic and Atmospheric Administration Climate Monitoring and Diagnostics Laboratory, and the University of Washington Quaternary Isotope Laboratory. This is a product of Project ARRCC (Analysis of Rapid and Recent Climate Change).

References

Andreae, M.O., Climatic effects of changing aerosol levels, in *Future Climates of the World: A Modeling Perspective*, edited by A. Henderson-Sellers, pp. 347-398, Elsevier Press, Amsterdam, 1995.

Barnola, J.M., D. Raynaud, Y.S. Korotkevich, and C. Lorius, Vostok ice core provides 160,000-year record of atmospheric CO_2, *Nature, 329*, 408-414, 1987.

Beer, J., U. Siegenthaler, G. Bonani, R.C. Finkel, H. Oeschger, M. Suter, and W. Wolfli, Information on past solar activity and geomagnetism from ^{10}Be in the Camp Century ice core, *Nature, 331*(6158), 675-679, 1988.

Beer, J., et al., Use of ^{10}Be in polar ice to trace the 11-year cycle of solar activity, *Nature, 347*, 164-166, 1990.

Beer, J., S.T. Baumgartner, B. Dittrick-Hannen, J. Hauenstein, P. Kubik, C. Lukasczyk, W. Mende, R. Stellmacher, and M. Suter, Solar variability traced by cosmogenic isotopes, in *The Sun As a Variable Star: Solar and Stellar Irradiance Variations*, edited by J.M. Pap, C. Frolich, H.S. Hudson, and S.K. Solanki, pp. 291-300, Cambridge Univ. Press, New York, 1994a.

Beer, J., F. Joos, C. Lukasczyk, W. Mende, J. Rodriguez, U. Siegenthaler, and R. Stellmacher, ^{10}Be as an indicator of solar variability and climate, in *The Solar Engine and Its Influence on Terrestrial Atmosphere and Climate*, edited by E. Nesme-Ribbes, pp. 221-233, Springer-Verlag, New York, 1994b.

Beer, J., W. Mender, R. Stellmacher, and O.R. White, Intercomparisons of proxies for past solar variability, in *Climatic Variations and Forcing Mechanisms of the Last 2000 Years*, edited by P.D. Jones, R.S. Bradley, and J. Jouzel, pp. 501-517, Springer-Verlag, New York, 1996.

Berger, A., and M.F. Loutre, Insolation values for the climate of the last 10 million years, *Quat. Sci. Rev., 10*, 297-317, 1991.

Cadle, R.D., C.S. Kiang, and J.F. Louis, The global scale dispersion of the eruption clouds from major volcanic eruptions, *J. Geophys. Res., 81*, 3125-3132, 1976.

Charlson, R.J., S.E. Schwartz, J.M. Hales, R.D. Cess, J.A. Coakley, J.E. Hansen, and D.J. Hofmann, Climate forcing by anthropogenic aerosols, *Science 255*, 423-430, 1992.

Clausen, H.B., and C.U. Hammer, The Laki and Tambora eruptions as revealed in Greenland ice cores from 11 locations, *Ann. Glaciol, 10*, 16-22, 1988.

Cole-Dai, J., L.G. Thompson, and E. Mosley-Thompson, A 485 year record of atmospheric chloride, nitrate and sulfate: Results of chemical analysis of ice cores from Dyer Plateau, Antarctic Peninsula, *Ann. Glaciol., 21*, 182-188, 1995.

Crowley, T.J., and K.-Y. Kim, Modeling the temperature response to forced climate change over the last six centuries, *Geophys. Res. Lett., 26* (13), 1901-1904, 1999.

Crowley, T.J., T.A. Criste, and N.R. Smith, Reassessment of Crete (Greenland) ice core acidity/volcanism link to climate change, *Geophys. Res. Lett., 20*(3), 209-212, 1993.

Curry, J.A., W.B. Rossow, D. Randal, and J.L. Schramm, Overview of Arctic cloud and radiation characteristics, *J. Clim., 9*, 1731-1764, 1996.

Dai, J., E. Mosley-Thompson, and L.G. Thompson, Ice core evidence for an explosive tropical volcanic eruption 6 years preceding Tambora, *J. Geophys. Res., 96*, 17,361-17,366, 1991.

Dlugokencky, E.J., P.M. Lang, K.A. Masarie, and L.P. Steele, Global CH_4 record from the NOAA/CMDL air sampling network, in *Trends '93: A Compendium of Data on Global Change*, edited by T.A. Boden, D.P. Kaiser, R.J. Sepanski, and F.W. Stoss, pp. 262-266, Carbon Dioxide Inf. Anal. Cent., Oak Ridge Nat. Lab., Oak Ridge, Tenn., 1994.

Eddy, J.A., The Maunder Minimum, *Science, 192*, 1189-1202, 1976.

Eddy, J.A., R.L. Gilliland, and D.V. Hoyt, Changes in the solar constant and climatic effects, *Nature, 300* (23/30), 689-693, 1982.

Etheridge, D.M., G.I. Pearman, and F. de Silva, Atmospheric trace-gas variations as revealed by air trapped in an ice core from Law Dome, Antarctica, *Ann. Glaciol., 10*, 28-33, 1988.

Etheridge, D.M., L.P. Steele, R.L. Langenfelds, R.J. Francey, J.-M. Barnola, and V.I. Morgan, Natural and anthropogenic changes in atmospheric CO_2 over the last 1000 years from air in Antarctic ice and firn, *J. Geophys. Res., 101*, 4115-4128, 1996.

Fiacco, R.J., T. Thordarson, M.S. Germani, S. Self, J.M. Palais, S. Whitlow, and P. Grootes, Atmospheric loading and transport due to the 1783-84 Laki eruption interpreted from ash particles and acidity in the GISP2 ice core, *Quat. Res., 42*, 231-240, 1994.

Franklin, B., Meteorological imaginations and conjectures, *Mem. Lit. Philos. Soc. Manchester, 2*, 357-361, 1784.

Free, M.P. and A. Robock, Global warming in the context of the Little Ice Age, *J. Geophys. Res., 104*, 19,057-19,070, 1999.

Hammer, C.U., H.B. Clausen, and W. Dansgaard, Greenland ice sheet evidence of post-glacial volcanism and its climatic impact, *Nature, 288*(5788), 230-235, 1980.

Hofman, D.J., Perturbations to the global atmosphere associated with the El Chichón volcanic eruption of 1982, *Rev. Geophys., 25* (4), 743-759, 1987.

Houghton, J.T., L.G. Meira-Filho, B.A. Callander, N. Harris, A. Kattenberg, and K. Maskell, *Climate Change 1995: The Science of Climate Change*, 572 pp., Cambridge Univ. Press, New York, 1996.

Hoyt, D.V., and K.H. Schatten, A discussion of plausible solar irradiance variations, 1700-1992, *J. Geophys. Ress, 98,* 18,895-18,906, 1993.

Keeling, C.D., and T.P. Whorf, Atmospheric CO_2 records from sites in the SIO air sampling network, in *Trends '93: A Compendium of Data on Global Change*, edited by T.A. Boden, D.P. Kaiser, R.J. Sepanski, and F.W. Stoss, pp. 16-26, Carbon Dioxide Inf. Anal. Cent., Oak Ridge Nat. Lab., Oak Ridge, Tenn., 1994.

Keen, R.A., Atmospheric effects, *Bull. Gl. Volc. Network, 22*, 15, 1997.

Khalil, M.A.K., and R.A. Rasmussen, Nitrous oxide trends and global mass balance over the last 3000 years, *Ann. Glaciol., 10*, 73-79, 1988.

Koch, D., D. Jacob, D. Rind, M. Chin, and I. Tegen, Tropospheric sulfur simulation in a GCM, *J. Geophys. Res., 104*, 23,799-23,822, 1999.

Lamb, H.H., Volcanic dust in the atmosphere, with a chronology and assessment of its meteorological significance, *Philos. Trans. R. Soc. London, 266*, 425-533, 1970.

Lamb, H.H., Supplementary volcanic dust veil assessments, *Clim. Monit., 6*, 57-67, 1977.

Lamb, H.H., Update of the chronology of assessments of the volcanic dust veil index, *Clim. Monit., 12*, 79-90, 1983.

Langner, J., and H. Rodhe, A global three-dimensional model of the tropospheric sulfur cycle, *J. Atmos. Chem., 13*, 225-263, 1991.

Langner, J., H. Rodhe, P.J. Crutzen, and P. Zimmerman, Anthropogenic influence on the distribution of tropospheric sulphate aerosol, *Nature, 359*, 712-716, 1992.

Lean, J., J. Beer, and R. Bradley, Reconstruction of solar irradiance since 1610: Implications for climate change, *Geophys. Res. Lett., 22*, 3195-3198, 1995.

Liousse, C., J.E. Penner, C. Chuang, J.J. Walton, H. Eddleman, and H. Cachier, A global three-dimensional model study of carbonaceous aerosols, *J. Geophys. Res., 101*, 19,411-19,432, 1996.

Lorius C., J. Jouzel, C. Ritz, L. Merlivat, N. I. Barkov, Y. S. Korotkevich, and V. M. Kotlyakov, A 150,000-year climatic record from Antarctic ice, *Nature, 316*, 591-596, 1985.

Mann, M.E., R.S. Bradley, and M.K. Hughes, Global-scale temperature patterns and climate forcing over the past six centuries, *Nature, 392*, 779-787, 1998.

Marland, G., R.J. Andres, and T.A. Boden, Global, regional, and national CO_2 emissions, in *Trends '93: A Compendium of Data on Global Change*, edited by T.A. Boden, D.P. Kaiser, R.J. Sepanski, and F.W. Stoss, pp. 505-584, Carbon Dioxide Inf. Anal. Cent., Oak Ridge Nat. Lab., Oak Ridge, Tenn., 1994.

Mitchell, J.F.B., and T.C. Johns, On modification of global warming by sulfate aerosols, *J. Clim., 10*, 245-267, 1997.

Mitchell, J.M., A preliminary evaluation of atmospheric pollution as a cause of the global temperature fluctuation of the last century, *Global Eff. Environ. Pollut.*, 139-155, 1970.

Moore, J.C., H. Narita, and N. Maeno, A continuous 770-year record of volcanic activity from East Antarctica, *J. Geophys. Res., 96*, 17,353-17,359, 1991.

Mosley-Thompson, E., L.G. Thompson, J. Dai, M. Davis, and P.N. Lin, Climate of the last 500 years: High resolution ice core records, *Quat. Sci. Rev., 12*, 419-430, 1993.

Nakazawa, T., T. Machida, M. Tanaka, Y. Fujii, S. Aoki, and O. Watanabe, Differences of the atmospheric CH_4 concentration between the Arctic and Antarctic regions in pre-industrial/pre-agricultural era, *Geophys. Res. Lett., 20* (10), 943-946, 1993.

Neftel, A., H. Oeschger, T. Staffelbach, and B. Stauffer, CO_2 record in the Byrd ice core 50,000-5,000 years BP, *Nature, 331*, 609-611, 1988.

Newhall, C.G., and S. Self, The volcanic explosivity index (VEI): an estimate of explosive magnitude for historical volcanism, *J. Geophys. Res., 87*, 1231-1238, 1982.

Overpeck, J.T., et al., Arctic environmental change of the last four centuries, *Science, 278,* 1251-1256, 1997.

Penner, J.E., R.E. Dickinson, and C.A. O'Neill, Effects of aerosol from biomass burning on the global radiation budget, *Science, 256,* 1432-1434, 1992.

Penner, J.E., R.J. Charlson, J.M. Hales, N.S. Laulainen, R. Leifer, T. Novakov, J. Ogren, L.F. Radke, S.E. Schwartz, and L. Travis, Quantifying and minimizing uncertainty of climate forcing by anthropogenic aerosols, *Bull. Am. Meteorol. Soc., 75*(3), 375-400, 1994.

Pollack, J.B., D. Rind, A. Lacis, J.E. Hansen, M. Sato, and R. Ruedy, GCM simulations of volcanic aerosol forcing, part I, Climate changes induced by steady-state perturbations, *J. Clim., 6*, 1719-1742, 1993.

Prinn, R.G., R.F. Weiss, F.N. Alyea, D.M. Cunnold, P.J. Fraser, P.G. Simmonds, A.J. Crawford, R.A. Rasumssen, and R.D. Rosen, Atmospheric CFC-11 (CCl_3F), CFC-12 (CCl_2F_2), and N_2O from the ALE/GAGE network, in *Trends '93: A Compendium of Data on Global Change*, edited by T.A. Boden, D.P. Kaiser, R.J. Sepanski, and F.W. Stoss, pp. 396-420, Carbon Dioxide Inf. Anal. Cent., Oak Ridge Nat. Lab., Oak Ridge, Tenn., 1994.

Raynaud, D., and J.M. Barnola, An Antarctic ice core reveals atmospheric CO_2 variations over the past few centuries, *Nature, 315,* 309-311, 1985.

Rind, D., The influence of vegetation on the hydrologic cycle in a global climate model, in *Climate Processes and Climate Sensitivity*, edited by J.E. Hansen, and T. Takahashi, pp. 73-91, AGU, Washington, D.C., 1984.

Rind, D., and J. Overpeck, Hypothesized causes of decade-to-century-scale climate variability: climate model results, *Quat. Sci. Rev., 12*, 357-374, 1993.

Rind, D., J. Lean, and R. Healy, Simulated time-dependent climate response to solar radiative forcing since 1600, *J. Geophys. Res., 104*, 1973-1990, 1999.

Robock, A., A latitudinally dependent volcanic dust veil index, and its effect on climate simulations, *J. Volcanol. Geotherm. Res., 11*, 67-80, 1981.

Robock, A., Volcanic eruptions and climate, *Rev. Geophys., 38,* 191-219, 2000.

Robock, A., and M.P. Free, Ice cores as an index of global volcanism from 1850 to the present, *J. Geophy. Res., 100*, 11,549-11,567, 1995.

Robock, A., and M.P. Free, The volcanic record in ice cores for the past 2000 years, in *Climatic Variations and Forcing Mechanisms for the Past 2000 Years,* edited by P.D. Jones and R.S. Bradley, pp. 533-546, Springer-Verlag, New York, 1996.

Robock, A., and H.-F. Graf, Effects of pre-industrial human activities on climate, *Chemosphere, 29*(5), 1087-1097, 1994.

Rose, W.I., Jr., Scavenging of volcanic aerosol by ash: Atmospheric and volcanologic implications, *Geology, 5*, 621-624, 1977.

Sato, M., J.E. Hansen, M.P. McCormick, and J.B. Pollack, Stratospheric aerosol optical depths, 1850-1990, *J. Geophys. Res., 98*, 22,987-22,994, 1993.

Schimel, D., et al., Radiative forcing of climate change, in *Climate Change 1995: The Science of Climate Change*, edited by J.T. Houghton, L.G. Meira Filho, B.A. Callander, N. Harris, A. Kattenberg, and K. Maskell, pp. 65-131, Cambridge Univ. Press, New York, 1996.

Self, S., M.R. Rampino, M.J. Carr, A reappraisal of the 1835 eruption of Cosiguina and its atmospheric impact, *Bull. Volcanol., 52*, 57-65, 1989.

Shindell, D.T., D. Rind, and P. Lonergan, Climate change and the middle atmosphere, part IV: Ozone response to doubled CO_2, *J. Clim., 11*, 895-918, 1998.

Sigurdsson, H., Evidence of volcanic loading of the atmosphere and climate response, *Palaeogeography, Palaeoclimatology, Palaeoecology, 89*, 277-289, 1990.

Simkin, T., and L. Siebert, *Volcanoes of the World*, 349 pp., Geosci. Press, Tucson, Ariz., 1994.

Solomon, S., R.W. Portmann, R.R. Garcia, W. Randel, F. Wu, R. Nagatani, J. Gleason, L. Thomason, L.R. Poole, and M.P. McCormick, Ozone depletion at mid-latitudes: Coupling of volcanic aerosols and temperature variability to anthropogenic chlorine, *Geophys. Res. Lett., 25*, 1871-1874, 1998.

Spruitt, H.C., Theoretical interpretation of solar and stellar irradiance variations, in *The Sun As a Variable Star: Solar and Stellar Irradiance Variations*, edited by J.M. Pap, C. Frolich, H.S. Hudson, and S.K. Solanki, pp. 270-279, Cambridge Univ. Press, New York, 1994.

Stothers, R.B., The great Tambora eruption in 1815 and its aftermath, *Science, 224*, 1191-1198, 1984.

Stothers, R.B., Major optical depth perturbations to the stratosphere from volcanic eruptions: Pyrheliometric period, 1881-1960, *J. Geophys. Res., 101*, 3901-3920, 1996.

Stuiver, M., Solar variability and climatic change during the current millennium, *Nature, 286*, 868-871, 1980.

Stuiver, M., and T.F. Braziunas, Atmospheric ^{14}C and century-scale solar oscillations, *Nature, 338*, 405-408, 1989.

Stuiver, M., and T.F. Braziunas, Sun, ocean, climate and atmospheric $^{14}CO_2$: An evaluation of causal and spectral relationships, *Holocene, 3*, 289-305, 1993.

Tegen, I. and I. Fung, Modeling of mineral dust in the atmosphere: Sources, transport, and optical thickness, *J. Geophy. Res., 99*, 22,897-22,914, 1994.

Tegen, I., A.A. Lacis, and I. Fung, The influence on climate forcing of mineral aerosols from disturbed soils, *Nature, 380*, 419-422, 1996.

Tegen, I., P. Hollrig, M. Chin, I. Fung, D. Jacob, and J. Penner, Contribution of different aerosol species to the global aerosol extinction optical thickness: Estimates from model results, *J. Geophys. Res., 102*, 23,895-23,915, 1997.

TEMPO, Potential role of vegetation feedback in the climate sensitivity of high-latitude regions: A case study at 6000 years B.P., *Global Biogeochem. Cycles, 10*(4), 727-736, 1996.

Thordarson, T., and S. Self, The Lake (Skaftar Fires) and Grimsvotn eruptions in 1783-1785, *Bull. Volcanol., 55*, 233-263, 1993.

Woodward, F.I., S.E. Lee, M. Lomas, and P. Cox, Dynamic vegetation within a world of changing climate, in *Global Analysis, Interpretation and Modeling: First Science Conference, International Geosphere-Biosphere Programme/Global Analysis, Interpretation, and Modeling*, Garmisch-Partenkirchen, Germany, 1995.

Yang, Q., P.A. Mayewski, S.I. Whitlow, M.S. Twickler, M.C. Morrison, R.W. Talbot, J.E. Dibb, and E. Linder, Global perspective of nitrate flux in ice cores, *J. Geophys. Res., 100*, 5113-5121, 1995.

Zardini, D., D. Raynaud, D. Scharffe, and W. Seiler, N_2O measurements of air extracted from Antarctic ice cores: Implication on atmospheric N_2O back to the last glacial-interglacial transition, *J. Atmos. Chem., 8*, 189-201, 1989.

Zielinski, G.A., Stratospheric loading and optical depth estimates of explosive volcanism over the last 2100 years derived from the Greenland Ice Sheet Project 2 ice core, *J. Geophys. Res., 100*, 20,937-20,955, 1995.

Zielinski, G.A., Use of paleo-records in determining variability within the volcanism-climate system, *Quat. Sci. Rev., 19*, 417-438, 2000.

Zielinski, G.A., P.A. Mayewski, L.D. Meeker, S. Whitlow, and M.S. Twickler, A 110,000-yr record of explosive volcanism from the GISP2 (Greenland) ice core, *Quat. Res., 45*, 109-118, 1996.

Zielinski, G.A., J.E. Dibb, Q. Yang, P.A. Mayewski, S. Whitlow, and M.S. Twickler, Assesment of the record of the 1982 El Chichón eruption as preserved in Greenland snow, *J. Geophys. Res., 102*, 30031-30045, 1997.

R. Healy, Woods Hole Oceanographic Institute, Woods Hole, MA 02543. (rhealy@whoi.edu)

D. Koch, D. Rind, and I. Tegen, NASA Goddard Institute for Space Studies, 2880 Broadway, New York, NY 10025. (dkoch@giss.nasa.gov; drind@giss.nasa.gov; itegen@giss.nasa.gov)

J. Lean, E.O. Hulburt Center for Space Research, Naval Research Laboratory, Washington, DC 20375. (lean@demeter.nrl.navy.mil)

E. Mosley-Thompson, Byrd Polar Research Center, The Ohio State University, 108 Scott Hall, 1090 Carmack Rd, Columbus, OH 43210. (thompson.4@osu.edu)

J.T. Overpeck, Institute for the Study of Planet Earth and Department of Geosciences, 715 N. Park Ave, 2nd Floor, University of Arizona, Tucson, AZ 85721 (jto@u.arizona.edu)

J. Penner, Department of Atmospheric, Oceanic, and Space Sciences, Space Research Building, University of Michigan, Ann Arbor, MI 48109. (penner@umich.edu)

A.D. Robertson, Institute of Arctic and Alpine Research and Department of Geological Sciences, University of Colorado, 1560 30th St, Boulder, CO 80303 (alexrob@email.arizona.edu)

G. Zielinski, Climate Studies Center, Institute for Quaternary Studies, University of Maine, Orono, ME 04469-5790. (gzielinski@maine.edu)

Received October 22, 1999; revised June 5, 2000;
accepted June 10, 2000.